

Added stresses because of the presence of FENE-P bead–spring chains in a random velocity field

By HESHMAT MASSAH† AND THOMAS J. HANRATTY

Civil Engineering Department, University of Illinois, Urbana, IL 61801, USA

(Received 20 February 1996 and in revised form 26 November 1996)

FENE-P bead–spring chains unravel in the presence of large enough velocity gradients. In a turbulent flow, this can result in intermittent added stresses and exchanges of energy between the chains and the fluid, whose magnitudes depend on the degree of unravelling and on the orientations of the bead–spring chains. These effects are studied by calculating the average behaviour at different times of an ensemble of chains, contained in a fluid particle that is moving around in a random velocity field obtained from direct numerical simulation of turbulent flow of a Newtonian fluid in a channel. The results are used to evaluate theoretical explanations of drag reduction observed in very dilute solutions of polymers.

In regions of the flow in which the energy exchange with the fluid is positive, the possibility arises that turbulence can be produced by mechanisms other than the interaction of Reynolds stresses and the mean velocity gradient field. Of particular interest, from the viewpoint of understanding polymer drag reduction, is the finding that the exchange is negative in velocity fields representative of the wall vortices that are large producers of turbulence. One can, therefore, postulate that polymers cause drag reduction by selectively changing the structures of eddies that produce Reynolds stresses. The intermittent appearance of large added shear stresses is consistent with the experimental finding of a stress deficit, whereby the total local shear stress is greater than the sum of the Reynolds stress and the time-averaged shear stress calculated from the time-averaged velocity gradient and the viscosity of the solvent.

1. Introduction

The addition of a high-molecular-weight polymer to a turbulent flow reduces the drag on a solid wall. A striking feature of this phenomenon is that it can occur at very low concentrations. For example, Walker, Tiederman & Luchik (1986) reported reductions of 20–30% for the flow of fully mixed water solutions of 1 to 3 p.p.m. of polyacrylamide through a 2.5×25 cm channel. Experiments in our laboratory with a fully mixed solution of 5 p.p.m. flowing in a 5.0×50 cm channel at a Reynolds number of 19000 (based on the half-height of the channel, the bulk velocity and the viscosity of water) show a reduction of about 50% from what would be observed for water. These results are consistent with earlier research by Patterson & Abernathy (1970) in a pipe and by Merrill *et al.* (1966) in a Couette viscometer. This paper is motivated by the need to understand the mechanism for drag reduction in studies such as those cited above.

Under equilibrium conditions the long-chain polymer molecules used for drag reduction are coiled. At the extremely low concentrations being considered they would be expected to show a small effect on the rheological properties of the solution if they

† Current address: Fluent Inc., 10 Cavendish Court, Lebanon, NH 03766, USA.

remained, approximately, in their equilibrium condition. However, the configuration of a polymer molecule can be affected by the flow and, if the reciprocal of the rate of strain is of the same order as the time constant of the polymers, the chain can unravel (Liu 1989; Wedgewood & Bird 1988). Under these conditions large additional stresses are introduced, even at very low concentrations of polymers. This is particularly evident in linear or planar extensional flows where large increases in viscosity are noted (Metzner & Metzner 1970; Lumley 1969, 1973; Lumley & Kubo 1984). Consequently, the suggestion by Lumley (1969) that uncoiling of polymer molecules, in the buffer region of a turbulent flow, causes drag reduction in very dilute solutions has had an important impact.

Lumley's theory has not been directly tested because of the difficulty of making laboratory measurements of the configuration of polymer molecules in a turbulent flow. This prompted a study of the behaviour of a solution of FENE-P bead-spring chains in a velocity field obtained from a direct numerical simulation (DNS) of turbulent flow of a Newtonian fluid in a channel (Massah *et al.* 1993). Fluid particles were tracked in the DNS and the changes of all of the components of the rate-of-strain tensor were noted. The response of an ensemble of chains to this changing velocity field was calculated. The concentration is considered small enough that interactions of the chains can be ignored; it is large enough that an average of the possible configurations due to Brownian motion may be considered.

The chains were found to unravel in the viscous sublayer to about 80% of their fully extended length, and to orient at an angle of about 4° to the direction of mean flow, when the time-averaged rate of shear at the wall was ten times the reciprocal time constant in the bead-spring model. In the buffer region the chains intermittently contracted, expanded and changed their orientation with respect to the mean flow. They remained contracted when they moved into the outer flow and uncoiled when they moved back into the buffer region. If a FENE-P bead-spring chain can represent the behaviour of a polymer molecule these calculations support the suggestion by Lumley that polymers can become unravelled by the turbulence in the buffer region. However, they differ in that Lumley did not anticipate an unravelling in the viscous sublayer. The calculated unravelling of a bead-spring chain in the viscous sublayer could explain the increased viscosity observed by Vissmann & Bewersdorff (1989) and by James, McLean & Saringer (1987) in elongational flow when a solution is pre-sheared in a laminar Couette or channel flow.

The influence of polymers on a turbulent flow will be felt through the introduction of additional stresses, associated with polymer stretching. These stresses have been studied by doing computational or laboratory experiments with simple rheological flows. However, uncertainties exist in applying the results to turbulence, which is three-dimensional, non-homogeneous and time-dependent. This prompted the present investigation of stresses introduced by FENE-P bead-spring chains in a velocity field obtained by a DNS of turbulent flow of a Newtonian fluid in a channel. This experiment cannot be realized in a laboratory, since the presence of polymer molecules would change the flow field. Therefore, the study may be considered to be a 'thought' experiment in which a given random velocity field is maintained and the stresses introduced by a dilute solution of bead-springs are determined; it is a rheological measurement in that stresses are determined for a prescribed velocity field. Calculations were done following the path of a fluid particle, so history was taken into consideration. Because of this and because of the elasticity of the springs, the solution is viscoelastic.

A computation in which polymer stresses are introduced back into the momentum equation is a far more difficult one, which may not be feasible with currently available

computers. In order to resolve the stress gradients, a few million fluid particles would have to be tracked. For a particle containing an ensemble of chains with five beads, fifteen minutes of CPU time on a Cray-2 would be used for each time step in the calculation. This would suggest that almost a century of CPU time would be needed on a Cray-2. Some possible simplifications of this calculation have been suggested by Wedgewood, Ostrov & Bird (1991), and some simplifications were explored by Massah (1993). A coarse grid was used and elastic dumbbells were fixed in space at the node points; that is, they did not follow fluid particles. Drag reduction was obtained but the calculated fluid turbulence was unrealistic.

Despite the limitations of the approach used in this paper, the calculations present some physical background that is needed to interpret findings about turbulent flows of very dilute polymer solutions for which polymer/polymer interactions can be ignored, if one accepts that a FENE-P bead–spring chain is a good representation of a polymer molecule. (The validity of the use of even the simple FENE-P dumbbell model is discussed by Wedgewood & Bird 1988.)

A number of reviews of laboratory studies of turbulent flows of polymer solutions have been presented. Therefore, it is only necessary to emphasize results which are particularly pertinent to this study. Very large velocity gradients exist in the viscous wall region (the viscous sublayer plus the buffer layer) close to a solid boundary. For large enough Reynolds numbers this region is thin so that its contribution to the velocity field can be described as an ‘effective slip’. The influence of drag-reducing polymers can be characterized as an increase in this effective slip caused by a thickening of the viscous wall layer (Virk 1975).

A well-documented structural feature of turbulence close to a flat wall is the existence of flow-oriented vortices with an average size of about 50 wall units (equal to the ratio of the kinematic viscosity, ν , to the friction velocity u^*). These vortices scale with the thickness of the viscous wall region and are associated with events making large contributions to the Reynolds stresses. The spanwise scale of the velocity fluctuations close to a wall increases with the addition of drag-reducing polymers, even if scaled with wall parameters defined for the drag-reduced flow (Fortuna & Hanratty 1972; Eckelman, Fortuna & Hanratty 1972; Massah 1993; Donahue, Tiederman & Reischmann 1972; Oldaker & Tiederman 1977). This can be interpreted as resulting from an increase in the size of the wall vortices or as a decrease in their importance.

Nikolaides (1984) and Lyons, Nikolaides & Hanratty (1988) used a two-and-a-half-dimensional model (three components of the velocity in two dimensions) to represent the flow-oriented wall vortices. Scaling arguments suggested that the characteristic period of these vortices when made dimensionless with respect to wall parameters should be approximately equal to the dimensionless characteristic wavelength, $T^+ \approx \lambda^+ \approx 100$. Luchik & Tiederman (1988) showed, for well-mixed polymer solutions, that an increase in λ^+ is accompanied by the same increase in T^+ . This suggests that these parameters are describing closely connected events.

Theoretical work aimed at understanding the influence of drag-reducing polymers has focused on how they could decrease the Reynolds stress by changing the characteristics of the turbulence. However, experiments with a central injection of a concentrated polymer thread (Bewersdorff 1984) show that the local shear stress calculated by a momentum balance, τ , is greater than the sum of the Reynolds shear stress and a viscous shear stress calculated with the solvent viscosity and the time-mean velocity gradient:

$$\tau > -\rho \overline{u'v'} + \mu_s \frac{d\bar{u}}{dy}. \quad (1)$$

Willmarth, Wei & Lee (1987) observed this effect in experiments in which the polymer was introduced into a settling chamber of their flow loop. This stress deficit has been carefully documented by Usui (1990) for poorly mixed polymers. Harder & Tiederman (see Tiederman 1990) also observed this stress deficit in their experiments with a well-mixed polyacrylamide solution at the highest strain rate at the wall (4000 s^{-1}) and the highest concentration (5 p.p.m.) that they studied. Koskie & Tiederman (1991) observed a stress deficit in the buffer region of a turbulent boundary-layer flow, with a well-mixed solution of polyacrylamide.

These studies show that polymers can introduce additional stresses other than would be expected from simple rheological experiments. A generally accepted explanation of this behaviour is not at present available. Berman (1989) used a FENE-P dumbbell model for the molecules to calculate an additional stress which depends on the time scale of the turbulent velocity fluctuations in the buffer region and on the elongational viscosity of the polymer solution, but not on the mean velocity gradient.

Laser Doppler velocimetry (LDV) (Willmarth *et al.* 1987; Tiederman 1990), particle-image velocimetry (PIV) (Massah 1993), and flush-mounted wall probes have been used to measure fluid turbulence in the presence of drag-reducing polymers. The first impression from PIV and LDV studies is that the turbulence is not strikingly different from what is found in a Newtonian flow. However, a closer examination of measurements reveals decreases in the magnitude of the normal and spanwise velocity fluctuations in the near-wall region, even when compared at the same friction velocity. For example, Fortuna & Hanratty (1972) used flush-mounted electrochemical probes to show that the ratio of the root-mean-square of the spanwise component of the velocity gradient at the wall to the time-mean velocity gradient is about one-half the value for a Newtonian fluid at a drag reduction of 50%. The LDV measurements of Tiederman (1990) reveal large decreases in the normal velocity fluctuations throughout the viscous wall region. These results seem consistent with the observation of an increase in the scale of the flow-oriented vortices that dominate the viscous wall region (Nikolaides 1984; Lyons *et al.* 1988). The striking decrease in the Reynolds stress correlation coefficient, observed by Luchik & Tiederman (1988), is not understood; it could be connected with a decrease in the importance of the highly coherent flow-oriented vortices.

Section 4 contains the principal contribution of this paper. The added stresses associated with the movement of FENE-P chains in a velocity field obtained from a direct numerical simulation of turbulent flow of a Newtonian fluid in a channel are presented under conditions that the ratio of the time-mean rate of strain at the wall to the reciprocal time constant in the model for the bead-spring chains is large enough that unravelling is occurring. By relating the changes of the stress to the changes in the rate-of-strain tensor, the rheology of solutions of FENE-P bead-spring chains in a random velocity field is studied. Several of the results are pertinent to experimental findings about drag-reducing polymers.

Large stresses and large exchanges of energy between the fluid and the bead-spring chains occur intermittently. These cannot be explained by introducing, intermittently, increases in viscosity. The bead-spring chains sense certain hydrodynamic events by unravelling and assuming a special orientation to the fluctuating flow field. Large losses of energy to the bead-spring chains appear to be associated with the flow-oriented vortices in the wall region and, therefore, could result in an increase in the scale of these vortices or a decrease in their importance. The occurrence of large intermittent shear stresses is consistent with the observation of stress deficits. The existence of a net

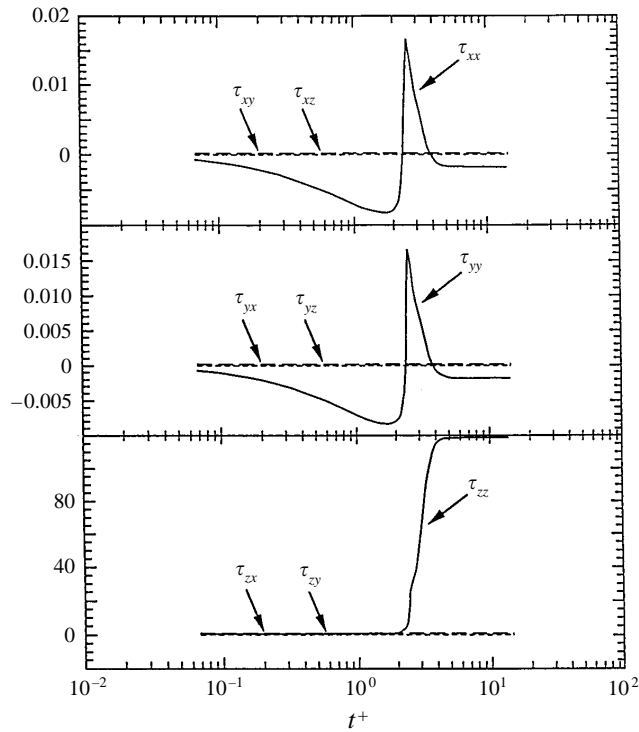


FIGURE 1. Added stresses (normalized with the largest principal stress in a Newtonian fluid) associated with a five-bead FENE-P chain in an extensional flow; $\lambda_p^+ = 10, b = 100$.

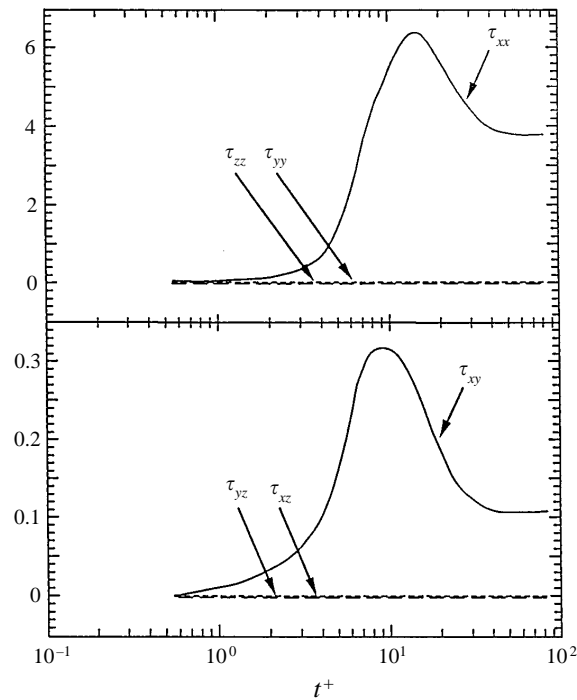


FIGURE 2. Added stresses (normalized with the largest principal to stress in a Newtonian fluid) associated with a five-bead FENE-P chain in a Couette flow; $\lambda_p^+ = 10, b = 100$.

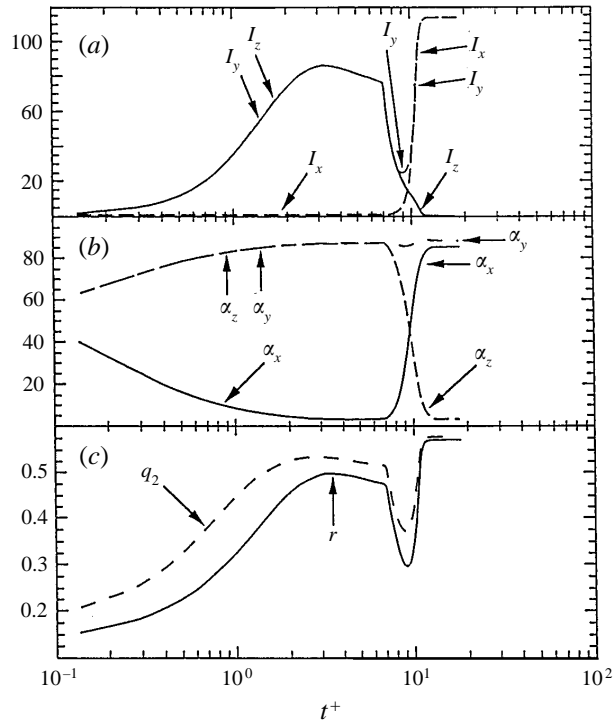


FIGURE 3. Configuration of a five-bead FENE-P chain in a Couette flow ($\partial u/\partial y = 1$) for $t^+ < 70$ and in a Couette flow plus an extensional flow in the z -direction ($\partial w/\partial z = 0.1, \partial u/\partial y = 1$) for $t^+ = 70-200$; $\lambda^+ = 10, b = 100$. (a) The moment of inertia about the i -axis; (b) the angle with the i -axis; (c) the length of link 2 and the distance between the end beads in the chain.

exchange of energy from the polymers to the turbulence in certain regions suggests the possibility that turbulence could be produced through polymer stresses.

Results on added stresses in several well-defined flow fields appear in §3. These are not central to the main thrust of the paper: they are presented to document the calculational procedure and to provide a basis for interpreting rheological behaviour in a random velocity field.

Before closing the introduction, a discussion of physical mechanisms other than the proposal by Lumley is appropriate. Metzner & Park (1964) showed that viscoelasticity is required for drag reduction to occur in solutions which are concentrated enough to show a non-Newtonian viscosity under simple shear. Seyer & Metzner (1969) suggested that viscoelasticity changes flow-oriented vortices because the polymer molecules would limit stretching motions and Gadd (1965) suggested that viscoelasticity would decrease the bursting frequency. Patterson & Abernathy (1970) argued that dissipation with a coiled polymer and work required for elastic deformation would contribute to high solution viscosity and oppose the intensification of vortices near the wall.

Several researchers have suggested that viscoelasticity can alter the turbulent velocity fluctuations. The most recent contribution of this type is from de Gennes (1990), who proposed that polymer effects will occur when the frequency of the velocity fluctuations is larger than a reciprocal time scale characterizing the elasticity of the polymer. Two scenarios, which depend on whether the polymer molecules are partially elongated or fully extended, are outlined. He suggested that polymers, in high enough concentrations, could affect the energy cascade by presenting an elastic limit to the

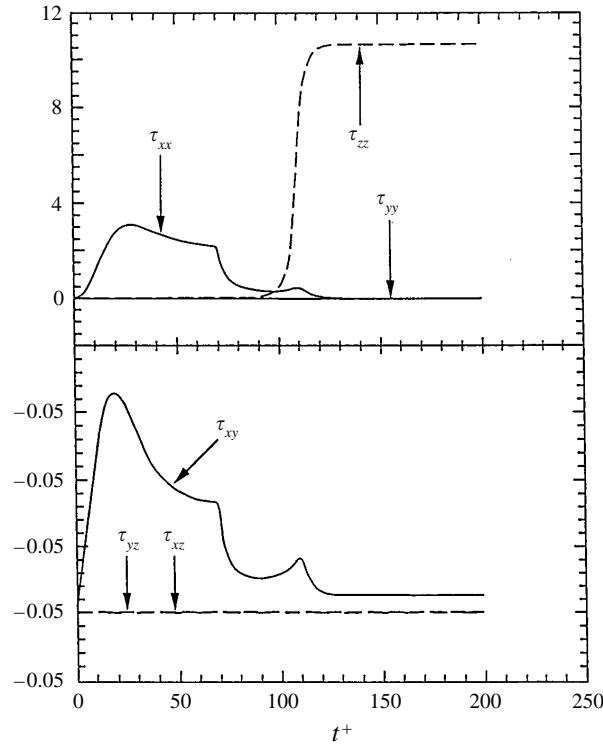


FIGURE 4. Stresses added by a five-bead FENE-P chain in a Couette flow ($\partial u/\partial y = 1$) for $t^+ < 70$ and in a Couette flow plus an extensional flow in the z -direction ($\partial w/\partial z = 0.1$) for $t^+ = 70$ –200; $\lambda^+ = 10$, $b = 100$.

frequency spectrum or by enhancing viscous dissipation at high frequencies. The possible impact of these effects on the velocity field is not clear.

Merrill *et al.* (1966) proposed that the alignment of polymers by a shear rate would give rise to anisotropic effects. Fortuna & Hanratty (1972) used this idea to explain their observed increase in the dimensionless spanwise scale, $\lambda v^*/\nu$, by arguing that spanwise shear rates see a larger viscosity than do the principal shear rates. Den Toonder (1996) has made a computer study of changes of the turbulence when viscous anisotropic effects are introduced.

2. Theory

The stresses generated by a pair of beads and the connecting spring are considered to be due to the tension or compression force transmitted through the spring and the momentum transfer of the beads due to Brownian motion. These effects are represented by the following equation given in Bird *et al.* (1987, pp. 88–89):

$$\tau^p = nH \frac{\langle \mathbf{Q}\mathbf{Q} \rangle}{1 - \langle Q^2/Q_0^2 \rangle} - \frac{b}{b+2} nkT\delta. \quad (2)$$

This considers an average of the possible configurations associated with Brownian motion. It employs Kramers' form of the polymer contribution to the stress tensor and the Peterlin approximation for $\langle \mathbf{Q}\mathbf{Q}/1 - (Q^2/Q_0^2) \rangle$. Equation (2) is used in all of the calculations presented in this paper. The first and second terms are, respectively, the

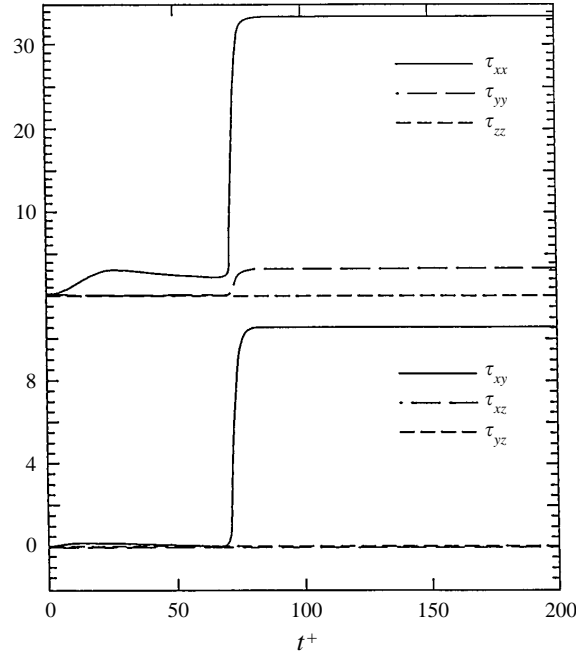


FIGURE 5. Stresses added by a five-bead FENE-P chain in a Couette flow ($\partial u/\partial y = 1$) for $t^+ < 70$ and in a Couette flow plus $\partial v/\partial x = 0.1$; for $t^+ = 70-200$; $\lambda^+ = 10$, $b = 100$.

contributions of the spring and the beads. A plus sign represents a tensile stress and a minus sign represents a compressive stress. The number of chains in a unit of volume is n ; H is the spring constant; \mathbf{Q} is the vector connecting two adjacent beads. This model allows a spring to be stretched to a maximum length of Q_0 . Equations describing the average dyadic product $\langle \mathbf{Q}\mathbf{Q} \rangle$ are given by Wedgewood & Bird (1988) and discussed in Massah *et al.* (1993). The non-dimensional term $b = HQ_0^2/kT$ is a measure of the extensibility of the chain, where k is the Boltzmann constant and T is the absolute temperature. The quantity δ is the unit tensor. For a chain with N beads, (2) is written as

$$\frac{\tau^p}{\rho u^{*2}} = \frac{nkT}{\rho u^{*2}} \left\{ b \left(\sum_{m=1}^{N-1} f_m \frac{\langle \mathbf{Q}_m \mathbf{Q}_m \rangle}{Q_0^2} \right) - \frac{(N-1)b}{b+2} \delta \right\}, \quad (3)$$

where $f_m = 1/1 - \langle Q_m^2/Q_0^2 \rangle$. The stress tensor is normalized with the wall shear stress, $\tau_w = \rho u^{*2}$, in turbulent flows, where u^* is the friction velocity. For results presented in §§3.1 and 3.2, ρu^{*2} is taken to be the largest principal strain rate multiplied by the solvent viscosity. For results in §3.3, ρu^{*2} is the dominant shear stress. The term $nkT/\rho u^{*2}$ may be interpreted as a dimensionless concentration. It is given a value of 0.003. This is specified by using $\rho = 1 \text{ g cm}^{-3}$, a molecular weight of 10^6 g mole^{-1} , a concentration of 1 p.p.m., a temperature of 22 °C, and a turbulent flow with $\rho u^{*2} = 10 \text{ g cm}^{-1} \text{ sec}^{-2}$. The shear rate at the wall would equal 10^3 s^{-1} . (The experiments in our laboratory cited in the Introduction were at a wall shear rate of $1.2 \times 10^3 \text{ s}^{-1}$. After the introduction of 5 p.p.m. of polymer the drag decreased to 50%, and the wall shear rate to $0.6 \times 10^3 \text{ s}^{-1}$.) Calculations were done for chains with five beads, for $b = 100$. A time constant for the chain is defined as $\lambda_p = \mathcal{S}/4H$, where \mathcal{S} is the Stokes drag coefficient for a single bead; it is a measure of the ratio of the force generated by Stokes drag on a bead to the strength of the spring. It was given a value of $\lambda_p^+ = 10$, where the + symbol is used to indicate that the quantity has been made dimensionless using u^* and

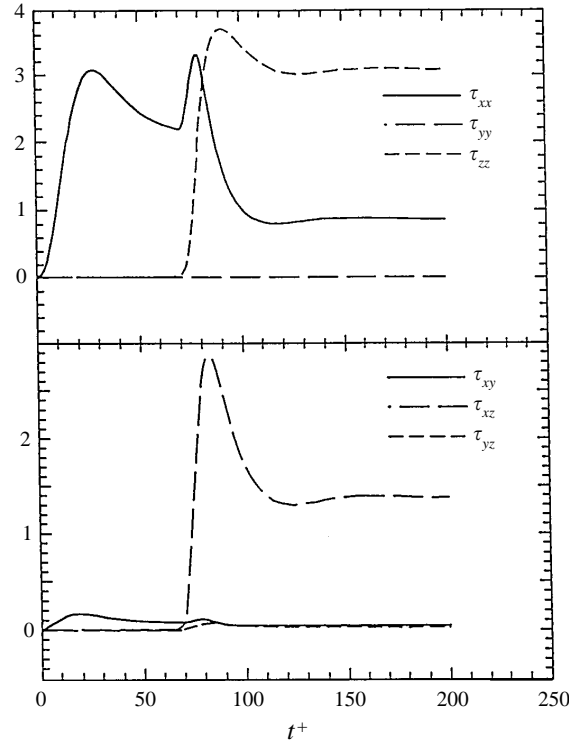


FIGURE 6. Stresses added by a five-bead FENE-P chain in a Couette flow ($\partial u/\partial y = 1$) for $t^+ < 70$ and in a Couette flow plus $\partial w/\partial x = 0.1$ for $t^+ = 70-200$; $\lambda^+ = 10, b = 100$.

ν . In the turbulent flow calculations the locations of a particle and the components of the velocity gradient tensor at that location were stored at 1020 time increments separated by $\Delta t^+ = 0.25$. The changes in the average configuration of the bead springs over each Δt^+ were calculated, for a realization of the velocity gradient tensor, in 357 time steps. A detailed description of the numerics is given by Massah *et al.* (1993). The evaluation of $\langle \mathbf{Q}_m \mathbf{Q}_m \rangle$ requires the solution of $(3N^2)/2$ (for even N) or $3(N^2 - 1)/2$ (for odd N) coupled ordinary differential equations. As N increases smaller time steps need to be used. Because calculated added stresses depend on the choice of $nkT/\rho u^{*2}$ and the number of springs, only the relative values of the different stresses are of interest.

Preliminary tests were done with chains having two, five and ten beads. The behaviour of a two-bead chain in simple flow is very close to that of a five-bead chain. The differences are in the magnitudes of the stretching and of the added stresses. However, in complex laminar flows and in turbulent flows, the behaviours of two-bead and five-bead chains are different. At certain times in these flows a five-bead chain creates added stresses that are not observed for a two-bead chain. Also, the ratios of the magnitudes of the stress components are different for five-bead and two-bead chains. However, the differences in the behaviours of five-bead and ten-bead chains are not important and consequently the enormous time required to do calculations with a ten-bead chain (compared to a five-bead chain) is not justified.

An equation of motion describing the velocity field can be obtained by representing the stress as a sum of the solvent stress, τ_{ij}^s , and the added stresses, defined by (3). A mechanical energy balance for the total kinetic energy of the turbulent velocity

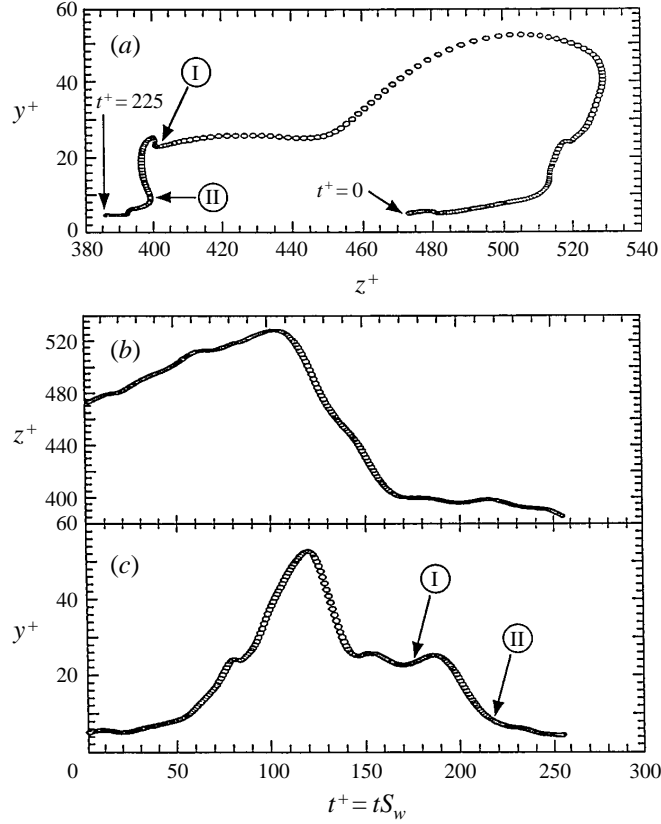


FIGURE 7. Trajectory of fluid particle 1, with location $y = 5, z = 475$ at $t^+ = 0$: (a) end view; (b) z versus time; (c) y versus time.

fluctuations can be derived by taking a moment of this equation, as described in Hinze (1987). A contribution of fluctuating solvent stresses is given by

$$\epsilon_v = \left(\frac{\partial u_i}{\partial x_j} + \frac{\partial u_j}{\partial x_i} \right) \frac{\partial u_i}{\partial x_j} = [\nabla \mathbf{u}' + \nabla \mathbf{u}'^T] : [\nabla \mathbf{u}'], \quad (4)$$

where all terms are made dimensionless with velocity u^* and length ν/u^* . Summation over the i and j indices is implied, \mathbf{u}' is the fluctuating velocity vector and the superscript T signifies the transpose. Equation (4) is always positive and represents the dissipation of mechanical energy due to viscosity. A consideration of the total energy balance for a Newtonian fluid (Hinze 1987) shows that this decrease in mechanical energy appears as an increase of the internal energy of the fluid (the temperature).

The contribution of the dimensionless fluctuating added stresses to $\tau_{ij}^p(\partial u_i/\partial x_j)$,

$$\epsilon_p = [\boldsymbol{\tau}^p] : [\nabla \mathbf{u}'], \quad (5)$$

will be called the 'added dissipation'. It differs from ϵ_v in that it may be positive or negative, since the springs have the possibility of extracting energy from or releasing energy to the fluid. This latter behaviour offers the possibility of observing a local instantaneous negative 'added dissipation', documented in the computation when $\boldsymbol{\tau}^p$ and $\nabla \mathbf{u}'$ do not have the same sign. This suggests the interesting possibility that energy can be withdrawn from the fluid in some parts of the flow and released in other parts.

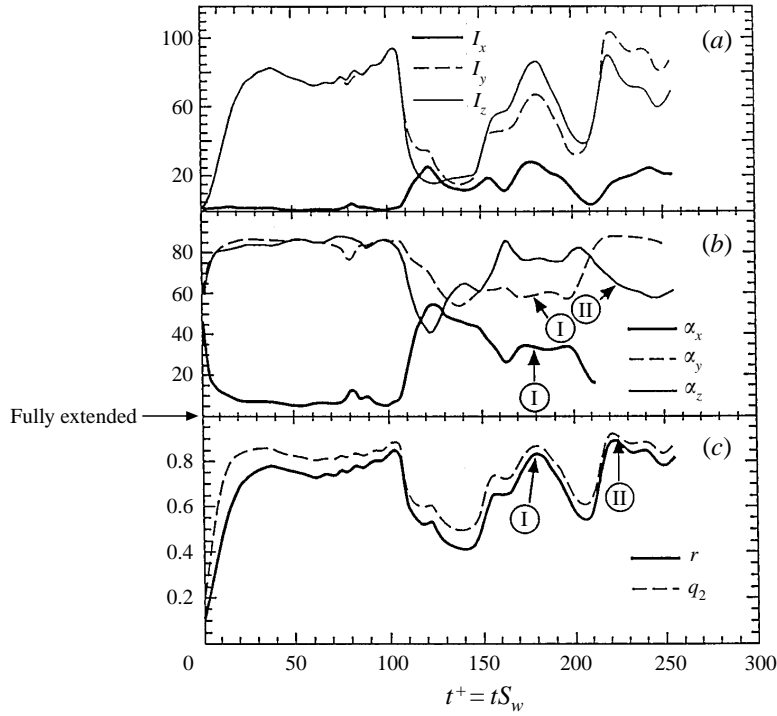


FIGURE 8. Variation of the configuration for particle 1. (a) Moments of inertia; (b) angles to the x -, y - and z -axes; (c) end-to-end distance and r.m.s. extension of link 2.

Consequently, it is not obvious how one should express an ‘average’ dissipation of turbulent energy due to the presence of FENE-P bead–spring chains because of the instantaneous possibility of energy storage within the chains. There is a precedent for using the analogue of (4) to deal with this problem (Bird *et al.* 1987, p. 106; Riseman & Kirkwood 1956), but the fluid temperature is not so simply related to ϵ_p and ϵ_v as for a Newtonian fluid (Appendix C of Curtiss & Bird 1991).

3. Results for defined flows

3.1. Uniaxial elongational flow

Figure 1 shows the stresses, normalized with the largest principal stress in a Newtonian fluid, caused by the presence of chains as a result of the inception of a uniaxial elongational flow in the z -direction at $t^+ = 0$, where time is normalized with the largest principal strain rate in the flow. As shown in figure 1 of Massah *et al.* (1993), the chains unravel to their maximum length and align along the z -axis. Therefore, only elongational stresses are produced. The major stress τ_{zz} is about 120 times the stress in a Newtonian flow. The very small values of τ_{yy} and τ_{xx} result from the Brownian motion of the beads. (This coil–stretch transition is discussed by Wiest *et al.* (1988) and Liu (1989).)

As the number of beads decreases the magnitudes of the stresses decrease. This decrease is not the same for all components of the stress tensor, but the shapes of the curves remain the same. The levels of the stresses increase with λ_p^+ ; for very small λ_p^+ no overshooting or undershooting was observed in the relations for τ_{yy} and τ_{xx} .

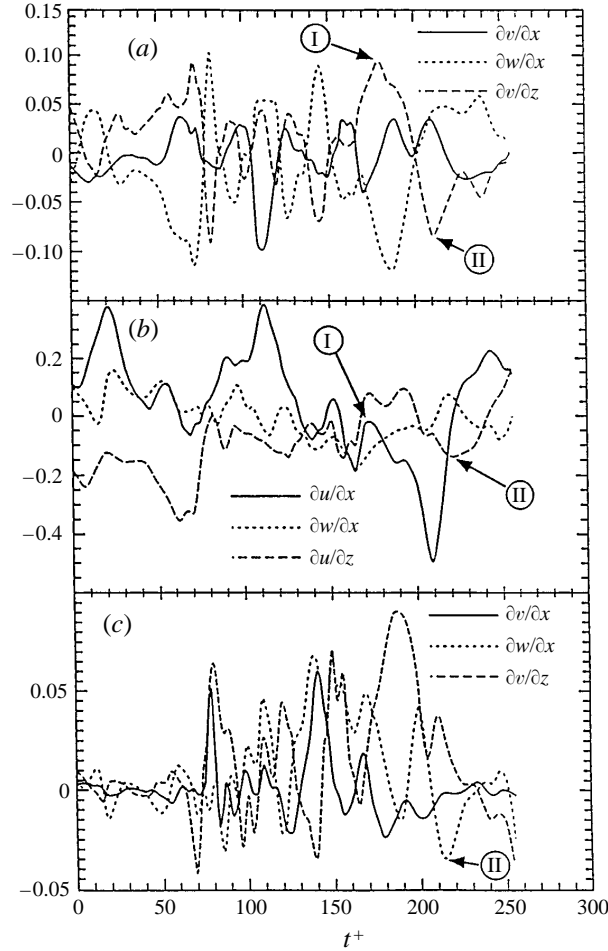


FIGURE 9. Variation of the components of the velocity gradient tensor, seen by particle 1.

3.2. Couette flow

Calculations for the added stresses due to the presence of bead–spring chains in a Couette flow are shown in figure 2. Again, these are normalized with the values of the maximum value of the principal stress in a Newtonian fluid. These were, therefore, done for a dimensionless rate of shear of $\partial u/\partial y = 2$, since the largest principal strain rate was selected to be the same as was explored in the preceding section. As already shown in Massah *et al.* (1993), a FENE-P bead–spring chain in this flow reaches about 80% of its full extension and orients at an angle of only 4° to the flow axis at $t^+ \approx 60$.

Both elongational ($\tau_{xx}, \tau_{yy}, \tau_{zz}$) and shear stresses (τ_{xy}) are produced. Stresses τ_{zz} and τ_{yy} are negative and negligible compared to τ_{xx} , which is positive. Overshoots in both τ_{xx} and τ_{xy} are observed. A steady state is reached in the Couette flow after $t^+ \approx 60$. The normal stress, τ_{xx} , is 3.8 times the largest principal stress because of the alignment of the bead–spring at a small angle to the flow direction; it is about 3% of the value shown in figure 1 because the chain does not extend fully, and because the velocity difference seen over the length of the chain is smaller. The value of added stress τ_{xy} is

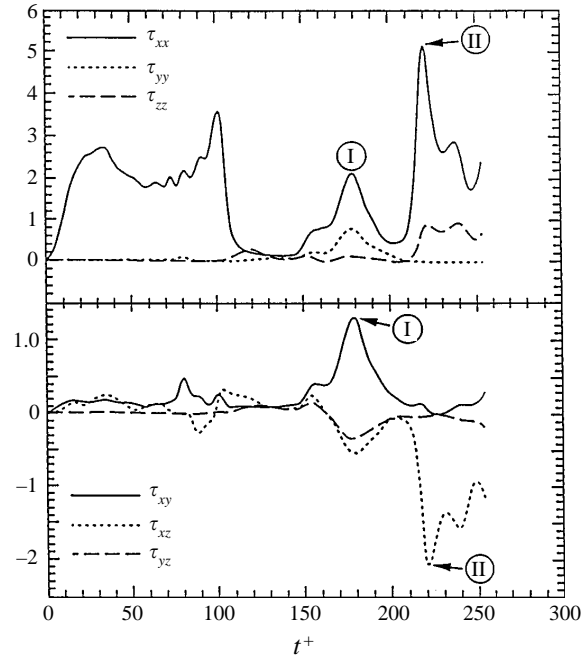


FIGURE 10. Added stresses for particle 1.

only 0.055 times the value for the solvent because of the small angle the chain makes with the x -axis.

Overshoots of the type shown in figure 2 have been previously calculated by Oettinger & Wedgewood (1988). Overshoots in the intrinsic viscosity have been observed in studies of the start-up of shear flows by Peterlin (1966) and by Mochimaru (1981).

3.3. Combined flow

Calculations in this subsection attempt to simulate what would happen to chains which are extended in the viscous sublayer of a turbulent field where $\partial u/\partial y \approx 1$ and then ejected into the buffer zone where they are exposed to a combination of other rates of strain in addition to a large $\partial u/\partial y$. Calculations of the components of the fluctuating velocity gradient tensor along the trajectory of a fluid particle in a random flow are shown in figure 9. The instantaneous $\partial u/\partial y$ is actually much larger in the viscous sublayer and in the buffer region because the time-mean $\partial u/\partial y$ needs to be added to the values given in the figure. These types of results motivated studies of the combined effect of $\partial u/\partial y$ and another velocity gradient whose magnitude is $0.1\partial u/\partial y$. Details of the calculations may be found in Massah (1993). A few examples are discussed here.

(a) Uniaxial extensions

Figure 3 shows the configurations of chains for a case in which $\partial u/\partial y = 1$ for $t^+ = 0-200$ and a uniaxial extension perpendicular to the plane of the shear ($\partial w/\partial z = 0.1$, $\partial v/\partial y = -0.05$, $\partial u/\partial x = -0.05$) is added for $t^+ = 70-200$. Figure 3(a) gives the moments of inertia, I_i , of the chain about the x -, y -, and z -axes, normalized with the equilibrium value. Figure 3(b) gives the angles, α_i , that the chains make with the x -, y - and z -axes. The distance between the end beads in the chain, r , and the length of the

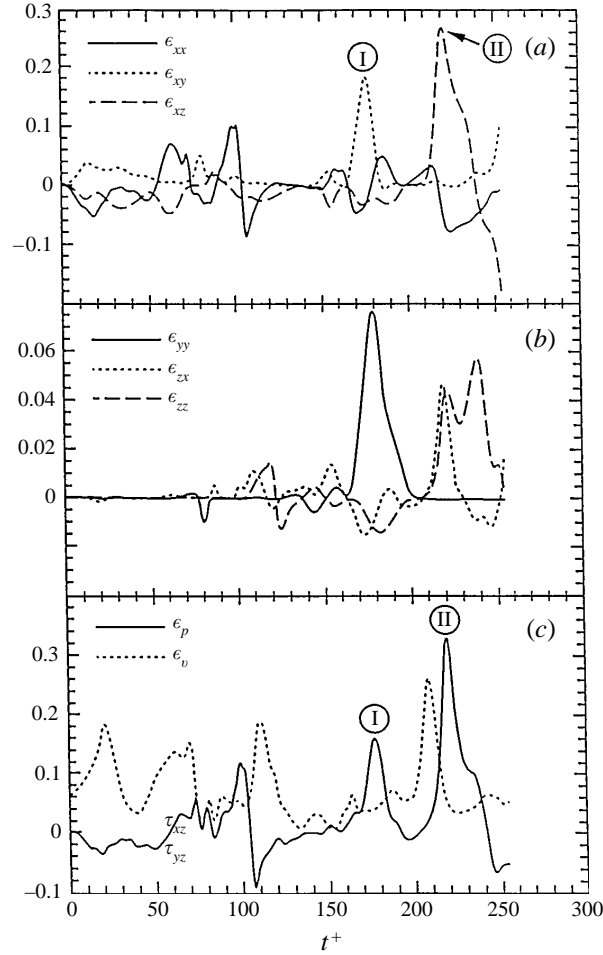


FIGURE 11. Energy dissipation following fluid particle 1: (a, b) components of the added energy dissipation, $\epsilon_{ij} = \tau_{ij}^p(\partial u_i/\partial x_j)$; (c) energy dissipation in the liquid, ϵ_p , and added energy dissipation associated with the presence of the particle.

second link, q_2 , are plotted in figure 3(c). Here the lengths, r and q_2 , are normalized with the maximum possible values, $(N-1)Q_0$ and Q_0 . The small positive value of $\partial w/\partial z$ that is introduced at $t^+ = 70$ causes the chain to recoil momentarily, to rotate off the x -axis and to align with the z -axis. The flow is then dominated by the $\partial w/\partial z$ component; the chains extend to a larger value than they had in the initial Couette flow. A period of $\Delta t^+ \approx 30$ is needed for the chain to reorient.

Figure 4 gives the added stresses generated by the chains. These are normalized with the shear stress that would exist in a Newtonian fluid with the dominant rate of shear. The addition of $\partial w/\partial z = 0.1$ causes τ_{zz} to increase to a value of 11 and τ_{xy} to decrease to a value of 0.01. Note that the added normal stress does not reach the value found in the calculations shown in figure 1, since $\partial w/\partial z$ is only one-tenth as large.

The introduction of a uniaxial extension in the plane of the shear and in the direction of the main flow ($\partial u/\partial x = 0.1$, $\partial v/\partial y = -0.05$, $\partial w/\partial z = -0.05$) for $t^+ = 70-200$ increases stretching in the x -direction and rotates the bead-spring closer to the x -axis. This results in a decrease in τ_{xy} and an increase in τ_{xx} .

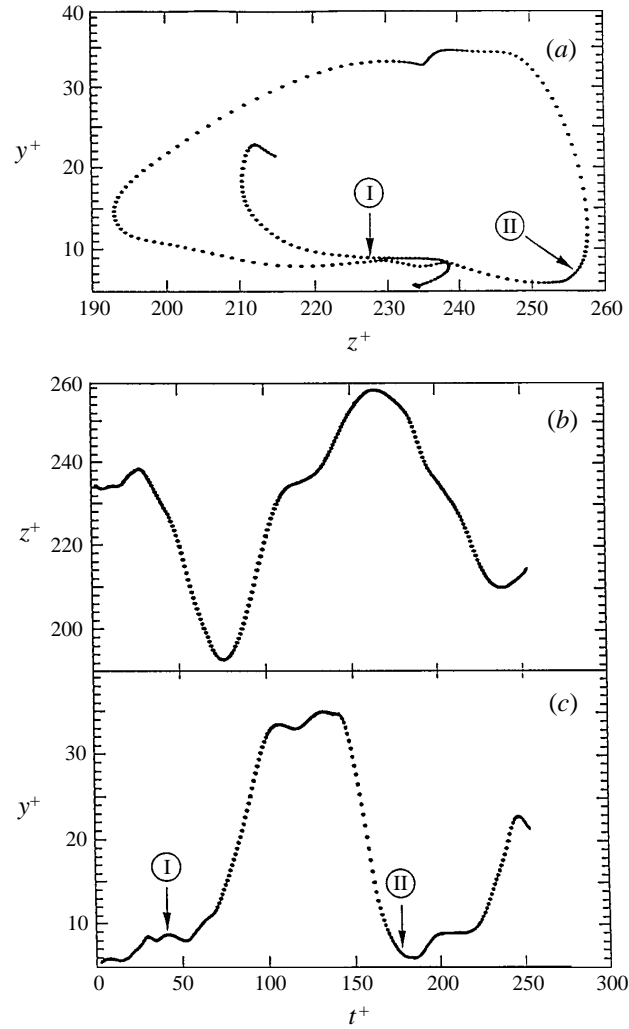


FIGURE 12. Trajectory of fluid particle 2.

The addition of a uniaxial extension in the plane of the shear and perpendicular to the direction of mean flow ($\partial v/\partial y = 0.1$, $\partial u/\partial x = -0.05$, $\partial w/\partial z = -0.05$) for $t^+ = 70$ – 200 has effects similar to what is observed with the addition of $\partial v/\partial x = 0.1$, to be discussed below. The chain is rotated toward the y -axis and stretched more than is observed for a Couette flow, with $\partial u/\partial y = 1$. Added stresses τ_{xx} and τ_{xy} respectively increase to 11 and 1.6. Of particular interest is the observation of a large added shear stress that could not be realized in a pure Couette flow and a large τ_{xx} in the presence of a negative $\partial u/\partial x$.

(b) *Two-dimensional extensions*

The influence of the imposition of a two-dimensional extension in the (y, z) -plane, on a shear flow, was studied by the introduction of ($\partial u/\partial x = -0.1$, $\partial v/\partial y = 0.05$, $\partial w/\partial z = 0.05$) at $t^+ = 70$. The chains collapse and reorient in the (y, z) -plane. The change in configuration is accompanied by increases in τ_{yz} , τ_{yy} and τ_{zz} .

The main effect of the introduction of a two-dimensional extension in the (x, z) -plane

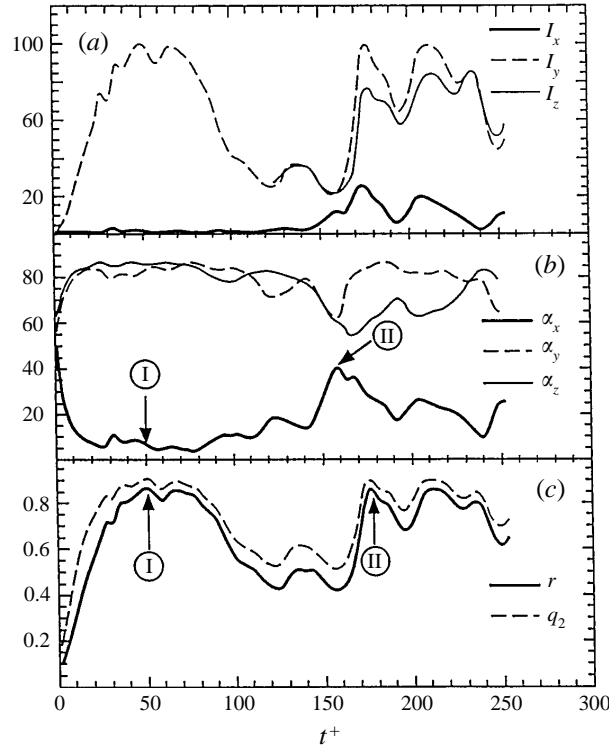


FIGURE 13. Variation of the configuration for particle 2: (a) moments of inertia; (b) angles to the x -, y - and z -axes; (c) end-to-end distance and r.m.s. extension of link 2.

($\partial v/\partial y = -0.1$, $\partial u/\partial x = 0.05$, $\partial w/\partial z = 0.05$) at $t^+ = 70$ is to cause the bead-spring chains to align close to the x -axis and to rotate slightly out of the (x, y) -plane. This results in a higher value of τ_{xx} ($= 5$) and very low value of τ_{xy} (≈ 0.01).

The introduction of a two-dimensional extension in the (x, y) -plane ($\partial w/\partial z = -0.1$, $\partial v/\partial y = 0.05$, $\partial u/\partial x = 0.05$) at $t^+ = 70$ causes increases in τ_{xx} , τ_{xy} and τ_{yy} .

(c) Shear rates in other planes

The principal effects of adding other velocity gradients (than extensional flows) to a shear flow are to rotate the bead-spring and to cause it to extend or contract. Results of calculations showing particularly large effects on the added stresses are shown in figures 5 and 6.

The addition of $\partial v/\partial x = 0.1$ (for $t^+ = 70-200$) to $\partial u/\partial y = 1$ increases stretching and changes the orientation to the x -axis from 4° to about 19° . As shown in figure 5, τ_{xx} increases to 33, τ_{xy} to 11 and τ_{yy} to about 3. The added shear stress is 200 times the added stress that would be observed in a simple Couette flow with the same $\partial u/\partial y$. An added stress τ_{xx} is observed which is about 1/3 of what would exist in a uniaxial flow with $\partial u/\partial x = 1$, even though $\partial u/\partial x = 0$. A relatively large τ_{yy} is realized, with $\partial v/\partial y = 0$.

The addition of $\partial w/\partial x = \pm 0.1$ (for $t^+ = 70-200$) to a flow with $\partial u/\partial y = 1$ causes slightly more stretching and a large rotation in the (x, z) -plane, so that the axes of the chains make an angle of 65° to the x -axis. As shown in figure 6, a positive $\partial w/\partial x$ results in large τ_{zz} (≈ 3) and τ_{xz} (≈ 1.5) and a reduction of τ_{xx} from 2 to about 0.9. A negative $\partial w/\partial x$ causes a negative value of τ_{xz} .

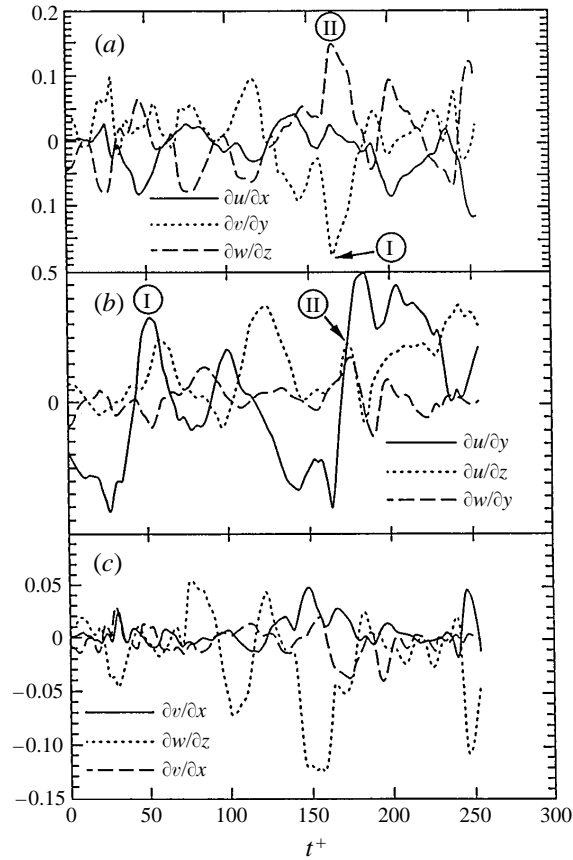


FIGURE 14. Variation of the velocity gradient tensor seen by particle 2.

The addition of velocity gradients $\partial u/\partial y$ or $\partial u/\partial z$ at $t^+ = 70$ has a small effect. The chain rotates toward the x -axis. The increase in τ_{xx} and decrease in τ_{xy} are smaller than what is found for the addition of a uniaxial stretching, $\partial u/\partial x$. The imposition of $\partial v/\partial x = -0.1$ at $t^+ = 70$ introduces an additional rotational motion in the (x, y) -plane. It has the opposite effect of $\partial v/\partial x = 0.1$: the chain collapses. The addition of $\partial v/\partial z = \pm 0.1$ at $t^+ = 70$ has no effect on the orientation of the chain and only a small effect on the stretching. Stresses τ_{xx} and τ_{xy} are doubled and τ_{yz} reaches a value of 0.1. A small increase in τ_{xz} (≈ 0.05) is observed.

3.4. Summary of results for defined flows

As is expected from laboratory experiments, a uniaxial stretching, which is large enough to extend chains fully, is associated with the appearance of a very large elongational stress. Extended bead–spring chains in a Couette flow are accompanied by a small added shear stress and by a large elongational stress, even though $\partial u/\partial x = 0$. These stresses appear because the chains are rotated around the z -axis. On average, they make a small angle to the x -axis and, therefore, see a velocity difference associated with the shear $\partial u/\partial y$. The shear stress added to a Couette flow by the presence of chains is about 3% of the added elongational stress and about 0.08% of the elongational stress added to a uniaxial elongational flow. Therefore, elongational viscosity is enhanced in both a Couette flow and an elongational flow. The small amount of shear viscosity added in a Couette flow may not be detectable in the laboratory.

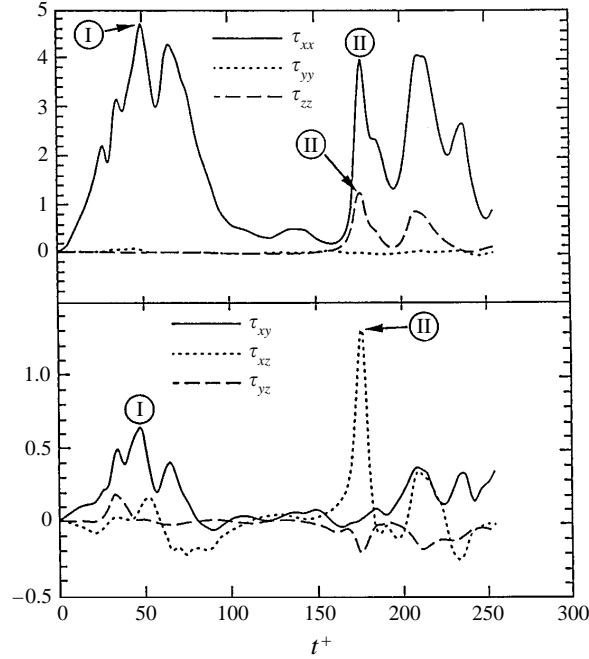


FIGURE 15. Added stresses for particle 2.

Calculations with a flow field consisting of the combination of a large shear, $\partial u/\partial y = 1$, and additional velocity gradients that are an order of magnitude smaller provide results which might not be anticipated from experiments with simple Couette or extensional flows. Thus the addition of $\partial v/\partial x = 0.1$ or of a uniaxial extension with $\partial v/\partial y = 0.1$, give added shear stresses, τ_{xy} , which are, respectively, 11 and 1.6 times the stress in the solvent. The addition of $\partial v/\partial x = 0.1$ causes the added elongational stress, τ_{xx} , to increase from 2 to 30 and elongational stress τ_{yy} to reach a value of 3, even though $\partial u/\partial x = 0$ and $\partial v/\partial y = 0$. The addition of a uniaxial extension in the (y, z) -plane ($\partial u/\partial x = -0.1$, $\partial v/\partial y = +0.05$, $\partial w/\partial z = +0.05$) introduces large values of the shear stresses, τ_{yz}, τ_{zy} , even though the shear rate in this plane is zero.

4. Results for a random flow field

4.1. Example 1

Figure 7 is an example of the trajectory of a fluid particle in a random field. The particle was released at the centre of the channel at $y^+ = 5$ and spent most of its time at the outer edge of the viscous sublayer and in the buffer region. The variation of the y - and z -positions with time are given in figure 7(b, c). Figure 7(a) gives an end view of the particle trajectory. The variation of the configuration of the chains with time is presented in figure 8, the components of the fluctuating velocity gradient, in figure 9, and the added stresses normalized with the average stress at the wall, in figure 10.

Figure 11(c) gives the energy dissipation due to viscosity in the fluid particle containing the chains, ϵ_p , and the 'dissipation' associated with the stresses added by the presence of the chains, ϵ_p . Figure 11(a, b) gives the contributions of the different components of the added stress to ϵ_p . Thus, $\epsilon_{ij} = \tau_{ij}^p (\partial u_i / \partial x_j)$, with no summation over the i and j indices. The complexity of these flows makes it difficult to interpret completely figures 10 and 11 from the time variation of the components of the velocity

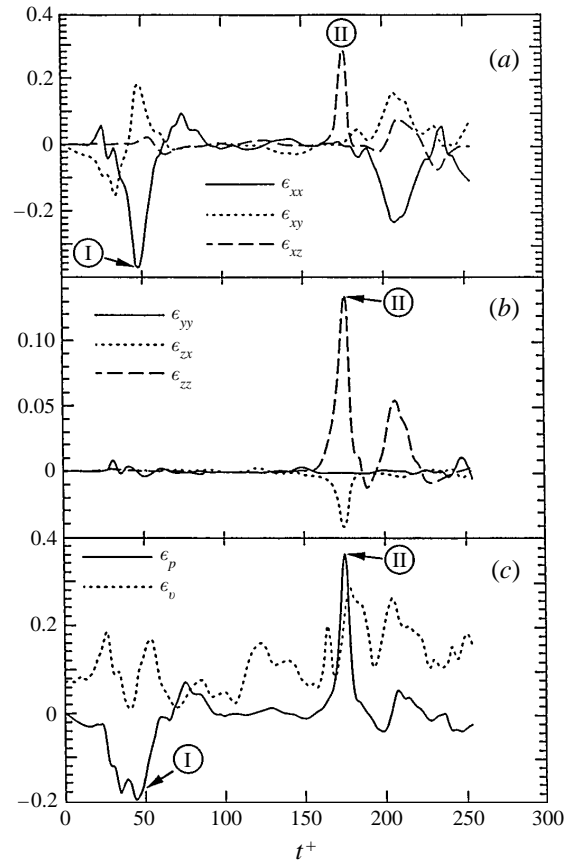


FIGURE 16. Energy dissipation associated with particle 2: (a, b) components of the added energy dissipation, $\epsilon_{ij} = \tau_{ij}^p (\partial u_i / \partial x_j)$; (c) energy dissipation in the fluid ϵ_p , and added energy dissipation associated with the presence of the particle.

gradient tensor, shown in figure 9. Nevertheless, some important features can be examined. In particular, the sharp peaks in ϵ_p at $t^+ = 178$ (position I) and at $t^+ = 220$ (position II) will be considered.

The configuration from $t^+ = 0-50$, shown in figure 8, is typical of the viscous sublayer. The behaviour is the same as for a Couette flow: the chains are at about 80% of their fully extended length and assume an angle of about 4° with the x -axis. The added stresses, τ_{xx} and τ_{xy} (shown in figure 10), are one-half those given in figure 2 because the normalizing stress in the Couette flow calculations was one-half the value used in these calculations. At $t^+ = 50-100$ the fluid particle moves rapidly out of the viscous sublayer and through the buffer layer. The polymer chains contained in the fluid particles keep approximately the same configurations they had in the sublayer; the large positive τ_{xx} is maintained. For $t^+ = 0-100$, the added energy dissipation associated with polymer stress τ_{xx} (ϵ_{xx} in figure 11) can be positive or negative, depending on the sign of $\partial u / \partial x$.

During the period $t^+ = 100-130$ the particle is outside the buffer layer where it experiences lower values of $\partial u / \partial y$ and a large negative value of $\partial u / \partial x$. The chains contract (figure 8) and create very small values of added stress (figure 10). At $t^+ = 150$ the particle moves back into the buffer region where the chains extend (figure 8, $t^+ = 180$), contract (figure 8, $t^+ = 205$) and change their orientation.

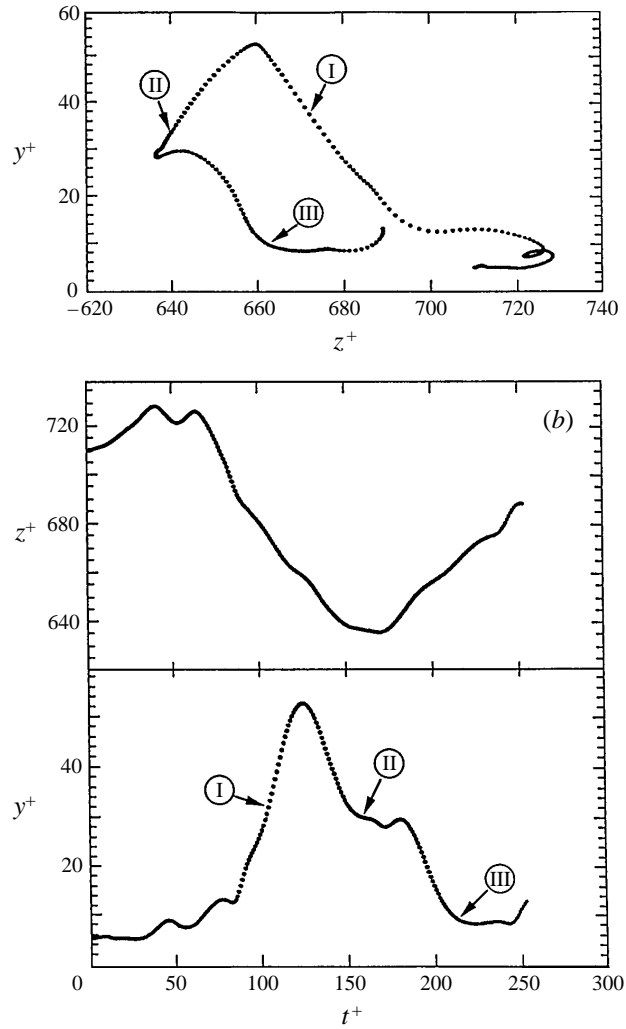


FIGURE 17. Trajectory of particle 3.

At position I there is a sudden change in direction (figure 7*a*) and a peak in $\partial v/\partial y$ (figure 9*a*). Figure 9(*b*) gives the fluctuations in $\partial u/\partial y$. The actual instantaneous value of this shear rate is the sum of the time-average and the fluctuations, so that it is relatively large. This, in combination with a large positive $\partial v/\partial y$ (and negative $\partial w/\partial z$) orients the extended chains in the (x, y) -plane at an angle of about 30° to the x -axis and of about 60° to the y -axis. As a consequence, large positive contributions by the chains to τ_{xy} and τ_{xx} arise (figure 10). The peak in ϵ_p , shown in figure 11, is mainly associated with $\tau_{xy} \partial u/\partial y$ (see ϵ_{xy} in figure 11*a*) since $\partial u/\partial x$ is small. The contraction of chains between $t^+ = 180$ and 200 appears to be associated with a decrease in $\partial u/\partial y$ and elongational strain rates ($\partial u/\partial y, \partial v/\partial y, \partial w/\partial z$) that are close to zero (figure 9*b*, $t^+ = 205$).

At II in figure 7 there is a sudden decrease in the velocity toward the wall and a change in the direction of motion. This is associated with an increase in $\partial u/\partial y$, positive values of $\partial u/\partial x$ and $\partial w/\partial z$, and negative values of $\partial v/\partial y, \partial w/\partial x, \partial u/\partial z$. The chains extend and reorient in the (x, z) -plane at an angle of about 60° to the z -axis. The

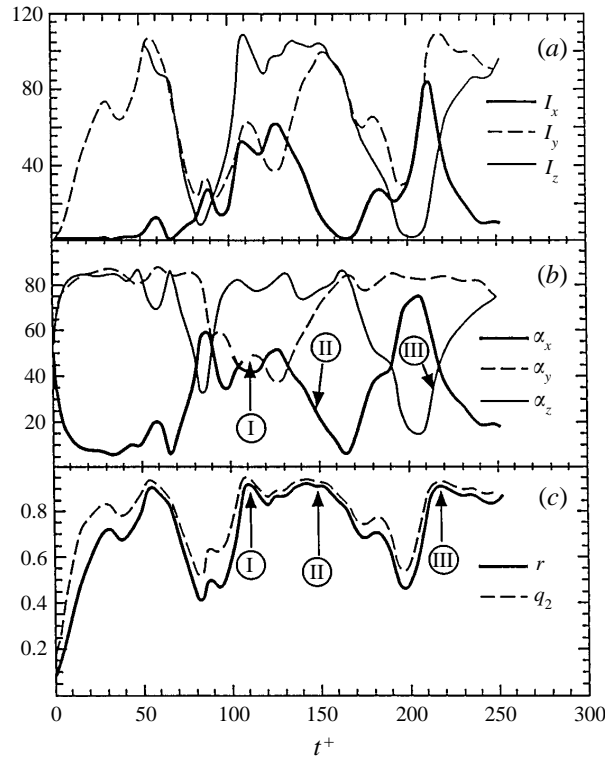


FIGURE 18. Variation of the configuration for particle 3: (a) moments of inertia; (b) angles to the x -, y - and z -axes; (c) end-to-end distance and r.m.s. extension of link 2.

experiments with combined fields suggest that the strong $\partial u/\partial y$ and the two-dimensional extension associated with a negative $\partial v/\partial y$ rotates the chains toward the x -axis and increases τ_{xx} . The shear rate $\partial w/\partial x$ rotates the chains in the negative z -direction where velocity differences exist over their lengths, due to the negative $\partial u/\partial z$. A large negative value of τ_{xz} and a large positive value of τ_{xx} result. The positive peak in ϵ_p is mainly the result of the interaction of a negative $\partial u/\partial z$ and a negative τ_{xz} (ϵ_{xz} in figure 11 *a*).

4.2. Example 2

Figures 12–16 present results for a particle which starts its trajectory at $y^+ = 5$ and spends most of its time in the buffer region.

At I the chains extend in the x -direction and make a small angle with the x -axis (figure 13) because of a large value of shear rate $\partial u/\partial y$ which is the sum of the time-averaged value and the fluctuation given in figure 14 (*b*). A large τ_{xx} (figure 15) results. This is associated with a negative ϵ_p at $t^+ = 5$ because $\partial u/\partial x$ is negative (figure 14 *a*).

Over the period $t^+ = 100$ –150 the particle is at $y = 35$, where the sum of the time-average and the fluctuations (figure 14 *b*) in $\partial u/\partial y$ are small. The chains are observed to contract (figure 13). At $t^+ = 150$ –170 the particle moves rapidly toward the wall where it experiences much larger time-averaged $\partial u/\partial y$. At position II the movement toward the wall is decelerated and there is an acceleration in the z -direction. The chains are exposed to a negative $\partial v/\partial y$ and large positive $\partial u/\partial z$ and $\partial w/\partial z$, in addition to large $\partial u/\partial y$. Since $\partial v/\partial y \approx -\partial w/\partial z$, this resembles a stagnation line (rather than a uniaxial extension) superimposed on a shear flow. The positive $\partial u/\partial y$ and $\partial u/\partial z$ unravel the

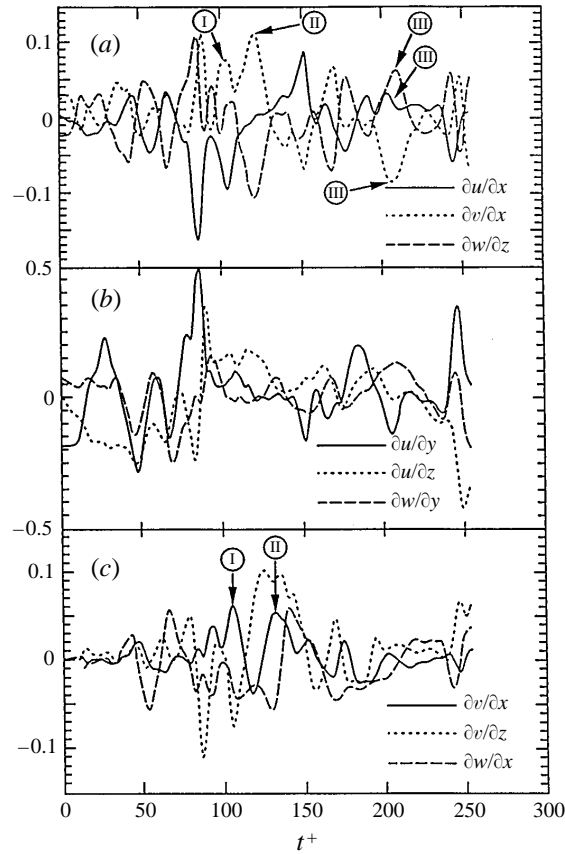


FIGURE 19. Variation of the velocity gradient tensor seen by particle 3.

chains and orient them along the x -axis; the positive $\partial w/\partial z$ stretches them further and rotates them into the (x, z) -plane, so that at $t^+ = 170$ – 180 they are at angles of 60° to the z -axis and 30° to the x -axis (figure 13). As a result, the chains contribute large τ_{xx} , τ_{zz} and τ_{xz} (figure 15). The peak in ϵ_p at $t = 175$ results from $\epsilon_{xz} = \tau_{xz} \partial u/\partial z$ and $\epsilon_{zz} = \tau_{zz} \partial w/\partial z$ (figure 16). Because $\partial u/\partial x$ is close to zero $\epsilon_{xx} = \tau_{xx} \partial u/\partial x$ makes a small contribution.

4.3. Example 3

Figures 17–21 give another example for which a particle starts at $y^+ = 5$ and spends most of its time in the buffer layer. Large positive ϵ_p are exhibited at I ($t^+ = 110$), II ($t^+ = 135$ – 160) and at III ($t^+ = 215$).

Over the period $t^+ = 0$ – 60 , for which the particle resides in the region $y^+ < 7$, an unravelling and alignment of the chains with the x -axis occurs because of large values of $\partial u/\partial y$. They reach a maximum extension of about 0.9 at $t^+ = 53$ (figure 18) when a large positive spike in τ_{xx} and a small negative spike in τ_{xz} are observed. The positive τ_{xx} makes a negative contribution to ϵ_p (figure 21a) and τ_{xz} makes a positive contribution (figure 21a).

Between $t^+ = 60$ and 100 the particle moves rapidly out of the viscous sublayer to the edge of the buffer region. The chains experience a large $\partial u/\partial y$, a large negative $\partial u/\partial x$ and positive $\partial v/\partial y, \partial w/\partial z$ of the same magnitude (figure 19). This results in

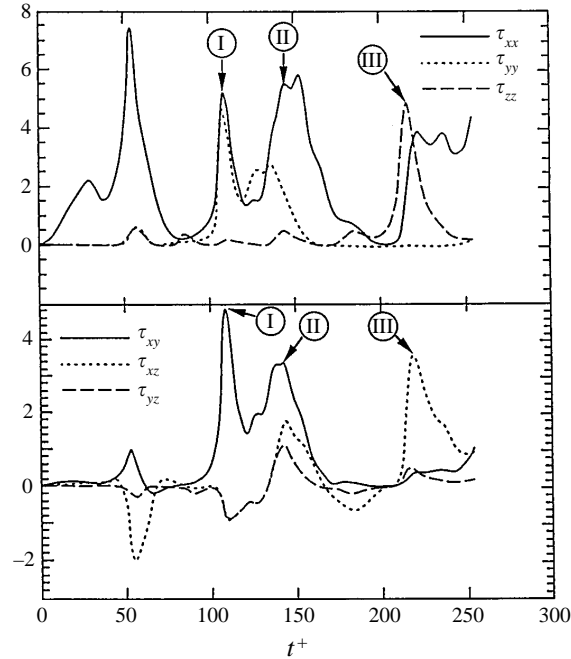


FIGURE 20. Added stresses for particle 3.

contracted chains which are not aligned with any of the axes (figure 18). As a result, the added stresses and ϵ_p are small.

Starting at $t^+ = 100$, the chains expand and orient in the (x, y) -plane at roughly 45° to the x - and y -axes (figure 18). Spikes in τ_{xx} , τ_{yy} and τ_{xy} are noted at $t^+ = 110$ where large positive values of $\partial v/\partial y$ and $\partial v/\partial x$, combined with $\partial u/\partial y$, produce a large difference in the streamwise and normal velocity components over the chain length. This results in positive values of $\tau_{xy} \partial u/\partial y$, $\tau_{yx} \partial v/\partial x$, $\tau_{yy} \partial v/\partial y$, a negative value of $\tau_{xx} \partial u/\partial x$ (because $\partial u/\partial x$ is negative) and a net positive peak in ϵ_p .

For $t^+ = 140$ – 170 , $\partial v/\partial y$ decreases and the chains orient with the x -axis (figure 18). Large values of τ_{xx} and τ_{xy} are noted in the transition ($t^+ = 140$ – 155), while $\partial u/\partial y \approx 0.08$ and the chains are not, yet, aligned with the x -axis. The peak in τ_{xy} at $t^+ = 135$ – 145 (figure 20) is associated with a peak in $\partial v/\partial x$ (figure 19c); the peak in τ_{xx} at $t^+ = 145$ – 155 (figure 20) appears to be related to a peak in $\partial u/\partial x$ and positive values of $\partial v/\partial x$, and $\partial u/\partial y$ (figure 19a). These stresses contribute to positive $\tau_{yx} \partial v/\partial x$, $\tau_{xx} \partial u/\partial x$ and a peak in ϵ_p , shown in figure 21(c) for $t^+ = 135$ – 160 .

Between $t^+ = 170$ and 200 a contraction and a rotation into the (x, z) -plane is observed. At $t^+ = 200$ – 220 the chains expand and orient along the z -axis. The peaks in τ_{zz} , τ_{xz} , and the peaks in ϵ_p at $t^+ = 215$ are caused by two-dimensional extension in the (x, z) -plane associated with positive $\partial w/\partial z$, $\partial u/\partial x$ and negative $\partial v/\partial y$ (see figure 19a).

4.4. Relation of large positive ϵ_p to the velocity field

Large values of τ_{xz} were observed for example 1, position I (1-I), example 2, position II (2-II), and example 3, position III (3-III). All of these events are characterized by large positive ϵ_p , large negative values of $\partial v/\partial y$ and a reorientation from the (x, y) -plane to the (y, z) -plane. $\partial w/\partial z$ and $\partial u/\partial x$ are positive and approximately equal. The flow involves a combination of a strong velocity gradient at the wall and a three-

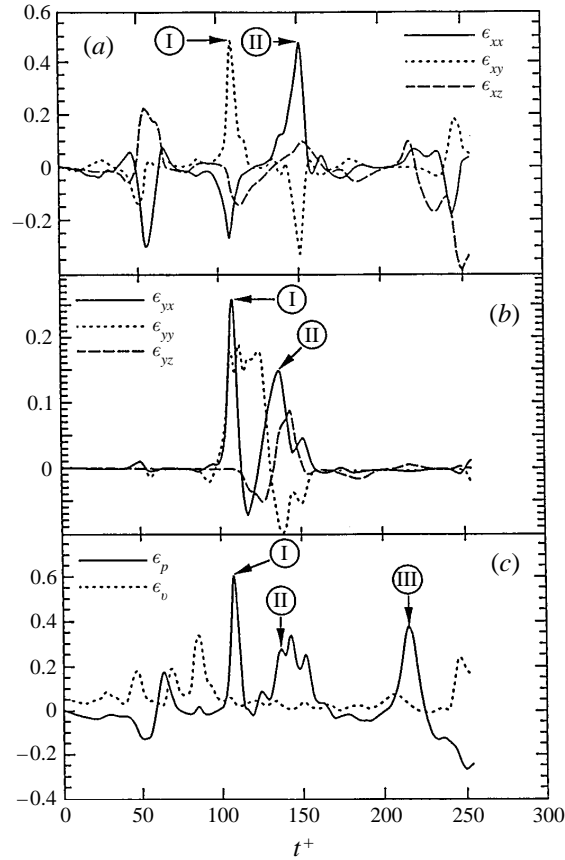


FIGURE 21. Energy dissipation associated with particle 3: (a, b) components of the added energy dissipation, $\epsilon_{ij} = \tau_{ij}^p(\partial u_i/\partial x_j)$; (c) energy dissipation in the fluid ϵ_v and energy dissipation associated with the presence of the particle ϵ_p .

dimensional extensional flow in the (x, z) -plane. Case (2-II) involves the combination of a strong velocity gradient, $\partial u/\partial y$, with a two-dimensional stagnation flow, negative $\partial v/\partial y$ and a positive $\partial w/\partial z$ of the same magnitude. Case (3-III) is a stagnation flow which is intermediate between cases 1 and 2.

An examination of the fluctuating velocity field indicates that these events are associated with the downwash of x -vortices. This is illustrated in figure 22(a), which shows the vectors in the (y, z) -plane at $t^+ = 165$. Position II of the particle being tracked in example 2 is indicated by the large dot at $y^+ = 10.9, z^+ = 257$. The x -vortex in which the particle is entrained has a spanwise dimension of 40–50 wall units and is typical of the structures identified in previous papers as being large producers of Reynolds stress.

Large values of τ_{xy} were observed for (1-I), (3-I) and (3-II). All are characterized by large positive $\partial v/\partial y$ at values of y^+ between 20 and 50 and associated with large τ_{xx} . As shown in figure 8, the chains are rotated away from the x -axis by the positive $\partial v/\partial y$ in case (1-I). For cases (3-I) and (3-II) rotation and stretching is aided by positive $\partial v/\partial x$ so the value of τ_{xy} is 6 times larger than for (1-I). Figures 22(b) and 22(c) show the vector field and the particle locations for points (1-I) and (3-I). Again, it is noted that large positive added dissipations are associated with x -vortices attached to the wall.

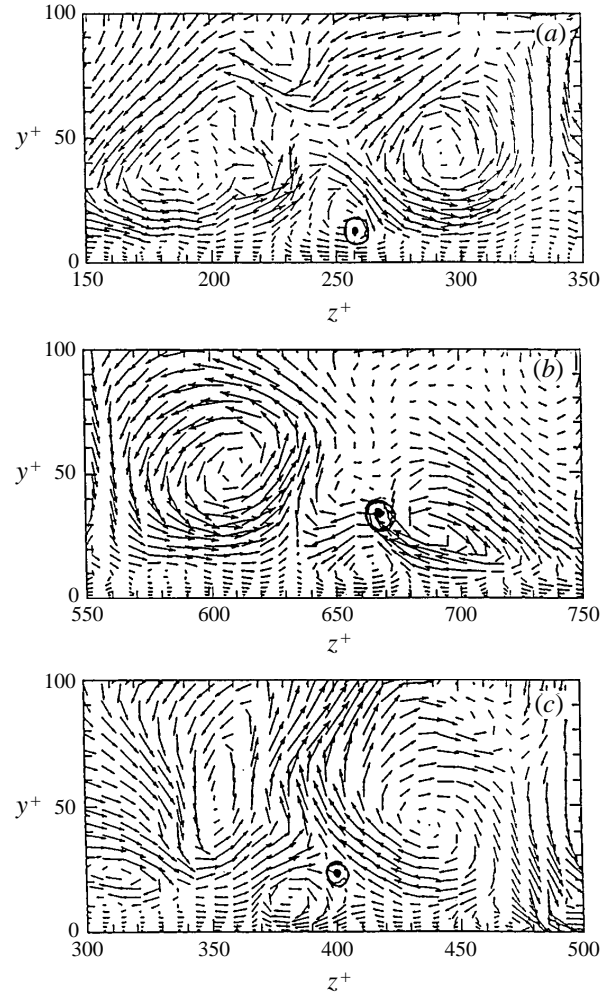


FIGURE 22. Velocity vector field associated with (a) particle position II in example 2, (b) particle position I in example 3, (c) particle position I in example 1. The enclosed dot is the position of the particle.

4.5. Summary of the results

Eight different fluid particles were tracked over a time interval of 250 units. The particles were released at different places in the channel. These studies provided added stresses for 8000 different realizations of the velocity gradient tensor in the presence of a concentration of bead–chains roughly equivalent to about 1 p.p.m. of polymer. The bottom wall is at $y^+ = 0$ and the centre of the channel is at $y^+ = 150$.

Figures 23 and 24 summarize calculations of τ_{ij} , ϵ_p and ϵ_v obtained for $y^+ < 60$. Beyond $y^+ = 50$ very small added stresses were generated. Data for the contributions of the different stress components to ϵ_p are given in figure 25.

Normal stresses were always positive, whereas shear stresses were positive or negative. For $y^+ < 20$ added stress τ_{xx} is dominant. Large values of τ_{zz} and τ_{xz} , observed around $y^+ \approx 10$, are caused by a reorientation of the chain into the (x, z) -

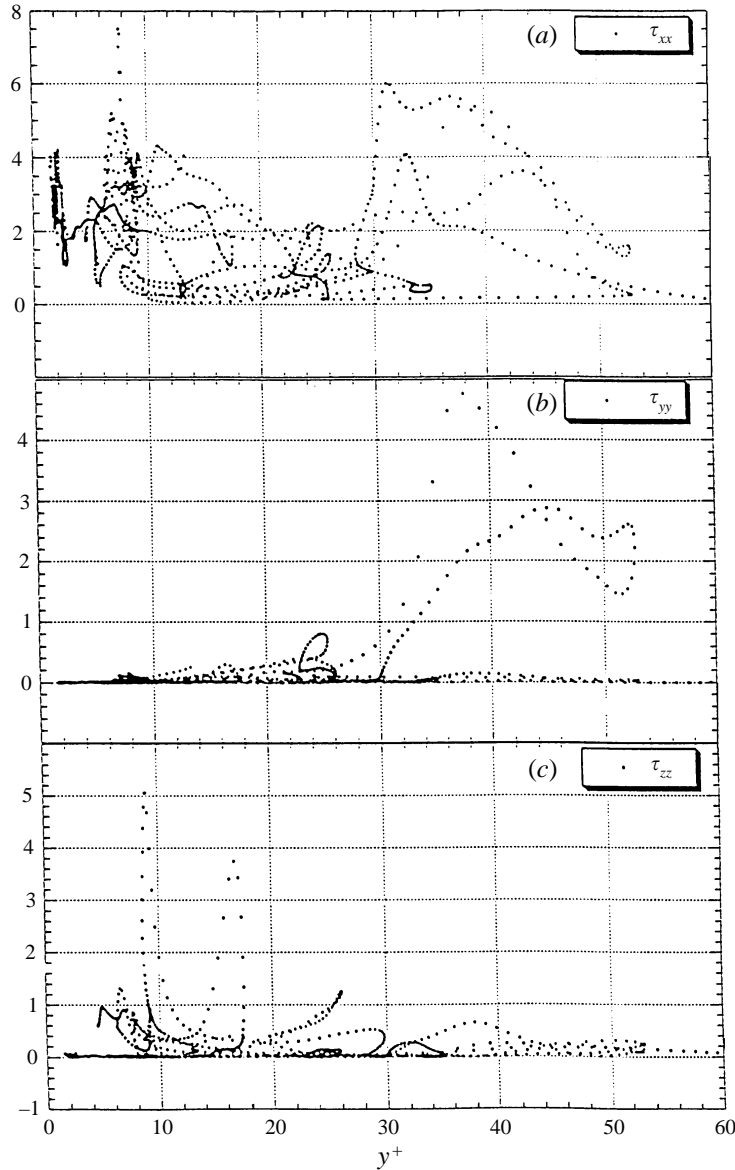


FIGURE 23 (a-c). For caption see facing page.

plane caused by impaction of fluid on the wall. Large values of τ_{xy} and τ_{yy} observed for $20 < y^+ < 50$ are associated with flow-oriented vortices.

Large negative spikes in ϵ_{xx} are observed at $y^+ = 10-20$. However, large positive and negative ϵ_{xx} are obtained for $y^+ > 30$. The largest value of positive dissipation was due to an added τ_{xy} at $y^+ = 30-40$ (point 3-I). For $y^+ = 30-40$ the added 'dissipation' is mainly positive. Near the wall, $y^+ < 10$, large positive and negative dissipations are observed. The net average values of ϵ_p over the whole region is positive.

The net average added shear stress, τ_{xy} , is positive. The peaks at $y^+ = 30-50$ are particularly large, being 3 to 5 times the wall shear stress.

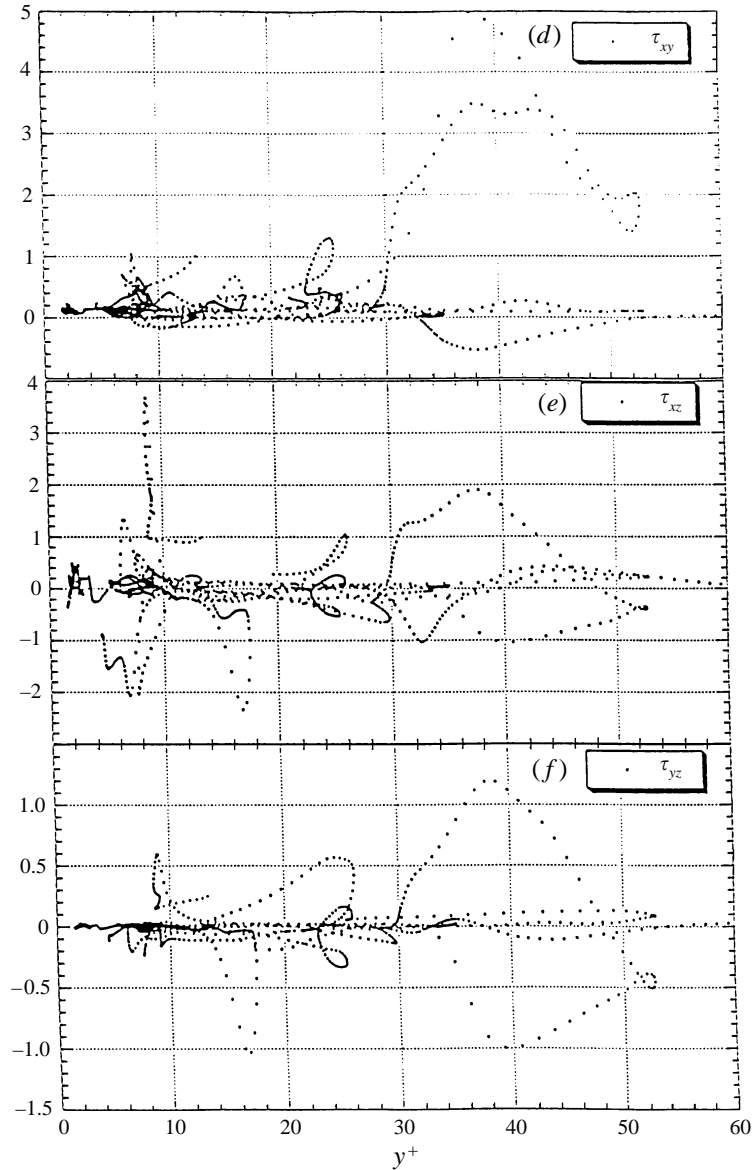


FIGURE 23. (a–f). Plots of added stresses calculated over the trajectories of eight particles.

5. Discussion of results on a random flow

5.1. Rheology of a FENE-P bead–spring chain in a random flow

In the viscous sublayer, FENE-P bead–spring chains behave similarly to what is found in a Couette flow. The chains are unravelled by the large velocity gradient, $\partial u/\partial y$. Because they are oriented very close to the x -axis the added shear stress, τ_{xy} , is small, of the order of 0.1. The added elongational stress, τ_{xx} , is large, but not so large as in a pure elongational flow.

When the particle moves out of the viscous sublayer the chains expand and contract, and change their orientation. Large added shear stresses, τ_{xy} and τ_{xz} , which would not be anticipated from simple rheological experiments, can develop. The interpretation of

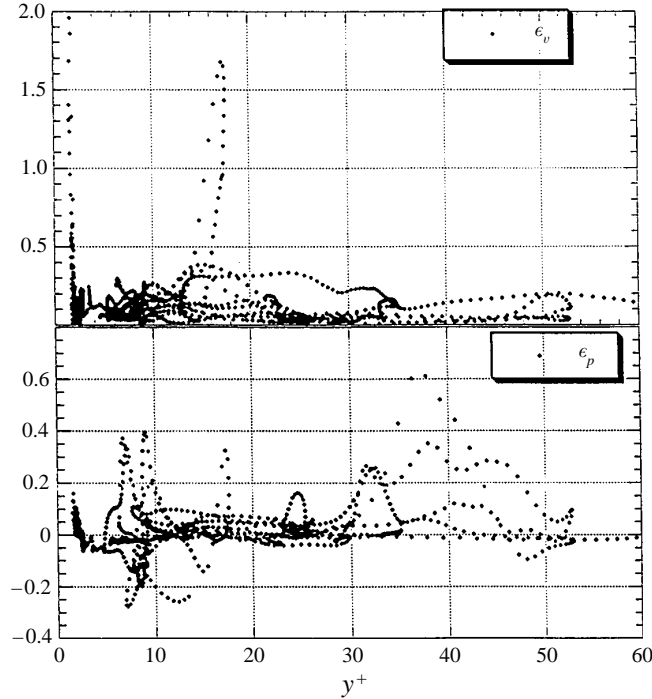


FIGURE 24. Plots of ϵ_v and ϵ_p calculated over the trajectories of eight particles.

these results in the outer part of the buffer region is complicated because a number of velocity gradient components have the same magnitude. Close to the wall, in the inner part of the buffer region, large values of τ_{xz} occur when the fluid impinges on the wall and the chain orients in the (x, z) -plane.

One of the more interesting results coming from this study is the observation of large intermittent non-isotropic ‘added dissipations’ which can be positive or negative, depending on whether energy is being transferred to the chain by the fluid or from the chain to the fluid. The complicated non-Newtonian rheology in a random flow is highlighted when it is observed that these events are not coincident with large dissipation of energy by the solvent; that is, they cannot be explained by simply changing the viscosity.

Only a few of the stresses contribute significantly to an energy exchange between the chains and the flow field. Elongational stress τ_{xx} is usually positive. Therefore, it produces turbulence when $\partial u/\partial x$ is negative and dissipates turbulence when $\partial u/\partial x$ is positive. Dissipation, associated with ϵ_{xx} , is mainly negative near the wall, $y^+ < 20$. For $20 < y^+ < 50$, ϵ_{xx} has both positive and negative peaks, but the positive ones are larger. The integral $\int \epsilon_{xx} dy^+$ over the whole field is positive, so that added stresses τ_{xx} are, on average, associated with the transfer of energy from the fluid to the bead-springs. Added shear stress τ_{xz} has both large positive and large negative values. It can be associated with positive and negative ϵ_p but, on average, is involved with a transfer of energy from the fluid to the bead-springs. Added stress τ_{xy} is mainly associated with a transfer of energy to the bead-springs from the turbulence since $\partial u/\partial y$ and τ_{xy} usually have the same sign. The average value of $\int \epsilon_p dy^+$ for all stress components is positive so there is an additional net dissipation of turbulent energy due to the presence of the bead-springs for the flow field that has been examined.

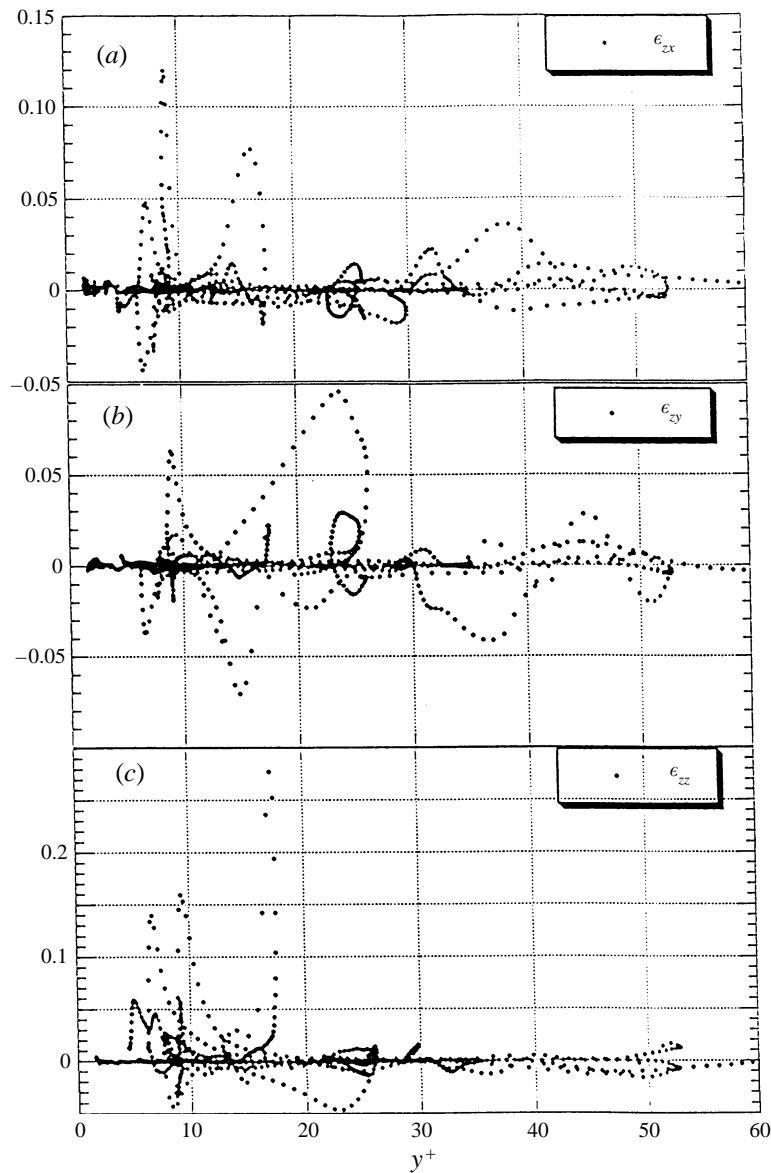


FIGURE 25 (a–c). For caption see page 97.

The observation that ϵ_{xx} for $y^+ < 20$ is, on average, negative indicates that polymer stresses are producing turbulence in this region. This could account, in part, for the large streamwise velocity fluctuations that are measured close to the wall. For another random field such as might exist for turbulent flows with a large amount of drag reduction, the possibility exists that the average ϵ_p is mostly negative so that polymer stresses could play a more important role than Reynolds stresses in producing turbulence.

5.2. Relevance to polymer drag reduction

The rheological results in this paper have a number of implications for theoretical work on drag reduction, if a FENE-P bead–spring chain is a good representation of a polymer molecule.

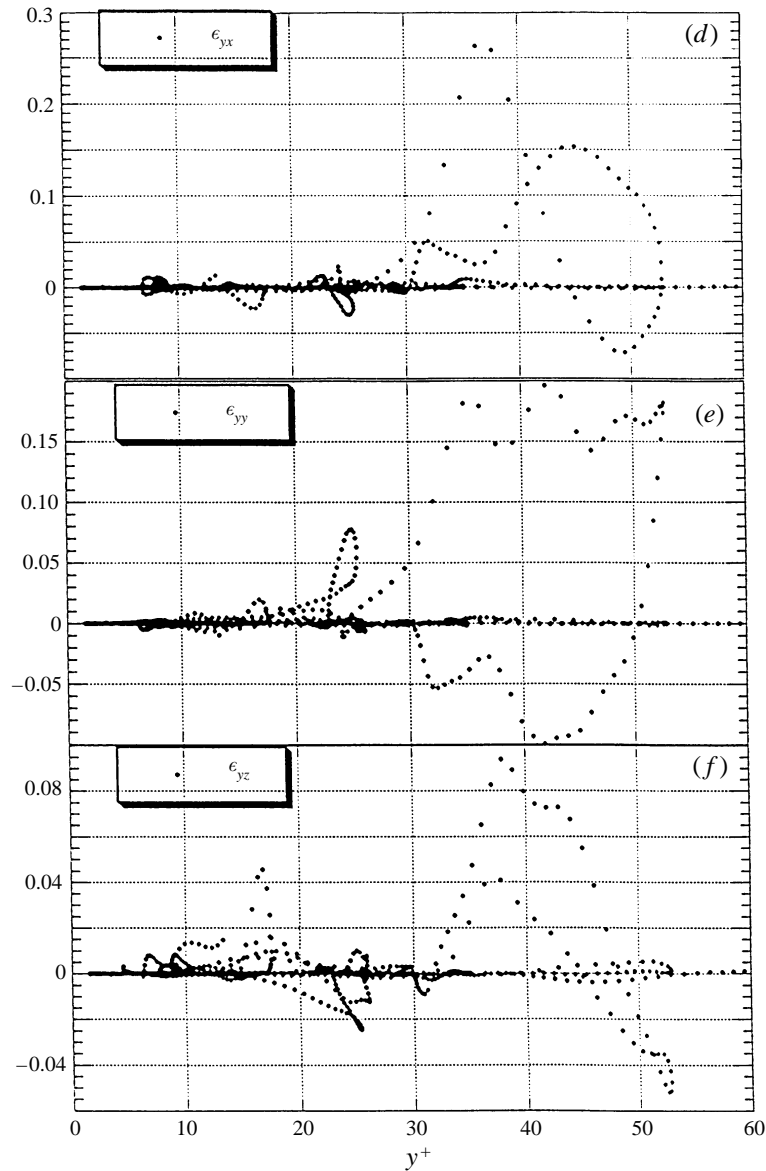
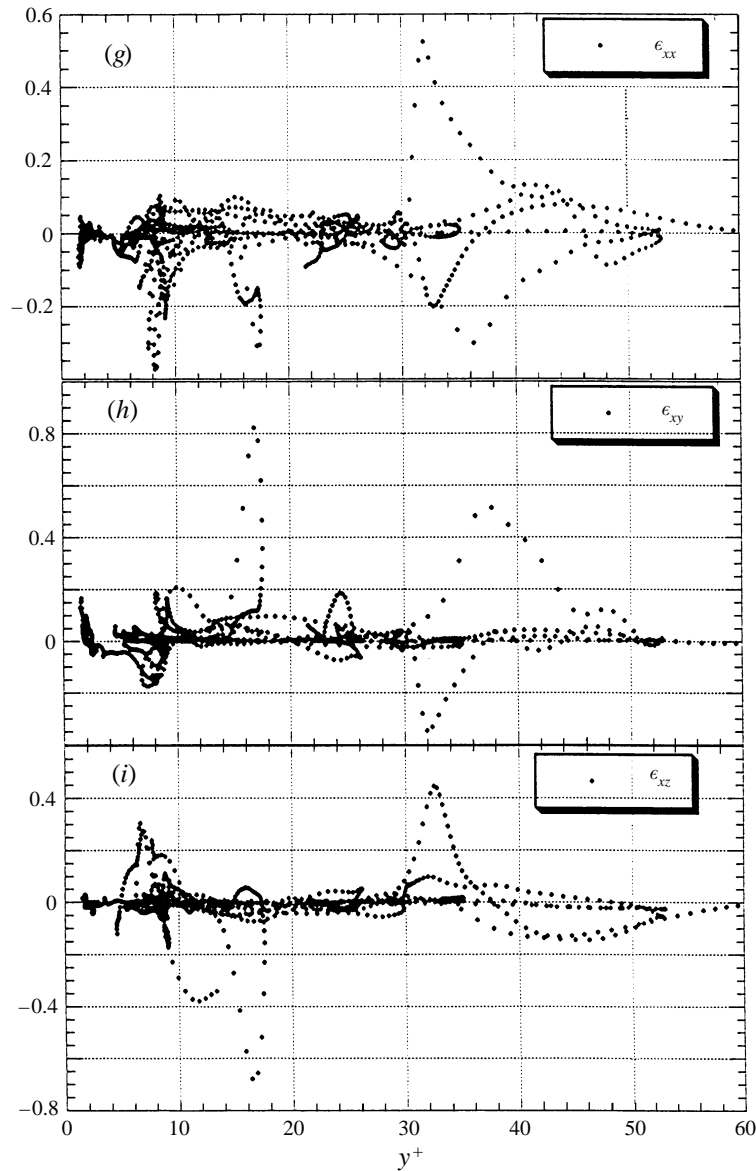


FIGURE 25 (*d-f*). For caption see facing page.

As pointed out in the preceding section, the added stresses that appear because of the presence of polymer molecules cannot be described by simply increasing the viscosity in the buffer region because these stresses are not directly related to the rate of strain in the same manner as for a Newtonian fluid. Furthermore, it is not evident to the authors that the observed relation between the added stresses and the velocity gradients can be explained by any simple constitutive equation.

There is some consistency of the results with theories that use the notion of an anisotropic viscosity, in that the added stresses are related to the orientation of extended polymer molecules. However, there are enough differences to have concerns about this approach. The assumption that stresses are related to velocity gradients in


 FIGURE 25. Contributions of the different stress components of ϵ_p .

the same way as for a Newtonian fluid seems to be inconsistent with the observation that peaks in ϵ_p and ϵ_v are not coincident. The only place in the field where there is a persistent orientation of polymer molecules is in the viscous sublayer. However, this configuration does not greatly enhance the stresses associated with either $\partial u/\partial y$ or $\partial w/\partial y$. The large values of τ_{xx} that exist in the viscous sublayer cannot be explained by an elongational viscosity since they are not associated with velocity gradient component $\partial u/\partial x$.

The observation of large viscosities in pure elongational flows of solutions of drag-reducing polymers has presented the interesting prospect that similar effects will be observed in turbulence. No direct evidence for this type of behaviour has been

obtained in this study. Elongational strains are always observed in conjunction with other components of the rate of strain tensor. The important effects of positive $\partial v/\partial y$ and positive $\partial w/\partial z$ come about because they rotate an extended chain away from the x -axis or out of the (x, y) -plane. The most important added normal stress, τ_{xx} , is mainly associated with large positive values of $\partial u/\partial y$ or a combination of $\partial u/\partial y$ and $\partial v/\partial x$.

The rheological study described in this paper agrees with the observation of a stress deficiency whereby the sum of the Reynolds shear stress and the time-averaged solvent stress is not equal to the total stress. Large intermittent values of τ_{xy} are observed in the buffer region when a certain combination of velocity gradient, components of roughly equal magnitude (such as $\partial v/\partial y$ and positive $\partial v/\partial x$ and $\partial u/\partial y$) extend the polymer chain and rotate it away from the x -axis.

The results appear to be most consistent with the argument (Seyer & Metzner 1969; Patterson & Abernathy 1970; Hanratty, Lyons & McLaughlin 1989) that polymers affect the development of flow-oriented vortices in the viscous wall layer. These vortices have an average spanwise dimension of 50 wall units ($\lambda^+ = 100$), and control the production of turbulence and the thickness of the viscous wall region. One of the striking laboratory findings about the effect of polymers on turbulence is an increase of λ^+ . The dimensionless streamwise velocity at the outer edge of the buffer layer, \bar{u}_0^+ , increases if λ^+ increases. Therefore, one approach to developing a theory of drag reduction is to understand why λ^+ increases. A possible explanation suggested by this study is that the increased dissipation (over that expected from viscous effects), associated with added stresses, could cause certain types of flow events to be dampened. Because of this, flow-oriented eddies in the viscous wall region with given length and time scales would have to increase in size (Hanratty *et al.* 1989) or become less prevalent.

Finally, it should be mentioned that the results of this study do not address a mechanism, discussed by de Gennes, that the energy cascade is affected because of the damping of high-frequency velocity oscillations. It is quite likely that such a phenomenon is operative. However, it is very difficult to connect this theory directly with drag reduction.

6. Conclusions

A study of the behaviour of FENE-P chains in a random flow reveals large intermittent stresses due to the presence of the chains and large intermittent exchanges of energy between the fluid and the chains, ϵ_p , which have been called ‘added dissipation’.

If a FENE-P chain is representative of a polymer molecule, these results suggest the following explanation for polymer drag reduction. When the ratio of the time constant of the polymer to the reciprocal of the rate of shear at the wall is large enough the polymers will unravel and introduce added stresses. These stresses can be associated with added dissipations, which can be positive or negative. Positive values of ϵ_p are found to be associated with the flow-oriented vortices in the viscous wall region that are large producers of Reynolds stress. Both scaling arguments and a calculation based on a two-and-a-half-dimensional model for the viscous wall region (Hanratty *et al.* 1989) suggest that an intermittent large added dissipation will result in an increase in the size of the wall vortices or a decrease in the fraction of the time that these vortices are present.

The presence of unravelled polymer molecules, therefore, causes an increase in the size (or a decrease in the importance) of the wall vortices in producing Reynolds

stresses and a possible contribution of an added time-averaged shear stress. A discussion of these results is facilitated by using simple eddy viscosity concepts (Mizushima & Usui 1977). If the change of stress in the viscous wall region can be ignored one can write

$$\tau_w = \tau^p + \tau^t + \tau^s, \quad (6)$$

where τ^p is a time-averaged added shear stress due to the presence of polymers, τ^t is the turbulent Reynolds stress

$$\tau^t = \nu_T \frac{d\bar{u}}{dy}, \quad (7)$$

and τ^s is the viscous stress due to the solvent

$$\tau^s = \nu \frac{d\bar{u}}{dy}. \quad (8)$$

If terms are made dimensionless with the solvent kinematic viscosity and the friction velocity $u^* = (\tau_w/\rho)^{1/2}$, one obtains

$$1 - \frac{\tau_p}{\tau_w} = \left(1 + \frac{\nu_T}{\nu}\right) \frac{d\bar{u}^+}{dy^+}. \quad (9)$$

If this is integrated out to the edge of the viscous wall region the velocity at y_0 is obtained as

$$\bar{u}_0^+ = \int_0^{y_0^+} (1 - \tau_p/\tau_w)(1 + \nu_T^+) dy^+. \quad (10)$$

If τ_p/τ_w were zero, an increase \bar{u}_0^+ (drag reduction) can be explained by a decrease of $\nu_T^+(y^+) = \nu_T/\nu$ caused by changes in the velocity field that result from an increase in λ^+ . However, if $\nu_T^+(y^+)$ is the same as for a Newtonian fluid finite values of τ_p/τ_w would give rise to a decrease in \bar{u}_0^+ , or a drag increase. Consequently, within this framework, the effect of a decrease in ν_T^+ needs to be larger than the effect of a drag defect $(1 - \tau_p/\tau_w)$.

A surprising aspect of laboratory measurements is that at large enough concentrations of polymers, the Reynolds stresses, τ^t , are too small to explain the level of turbulence by the mechanism observed in solvent flow, $-\tau_t d\bar{u}/dy$. The calculations presented in this paper suggest that, under these circumstances, the fluctuating polymer stresses could produce turbulence because of the existence of a net negative value of ϵ_p . This presents an interesting physical picture of a production mechanism whereby the mean flow transfers energy to polymers. Part of this energy will be directly transferred into heat through τ_p . However, another part, associated with fluctuations in the polymer stresses, is transferred to turbulent velocity fluctuations which, in turn, dissipate into heat.

H. Massah gratefully acknowledges discussions with Professor J. P. Murtha of the Civil Engineering Department, University of Illinois, Urbana. The work was supported by the Petroleum Research Fund of the American Chemical Society and the National Science Foundation under Grant NSF CTS 95-00518. We also acknowledge the support and the facilities of the National Center for Supercomputing Applications at the University of Illinois, Urbana.

REFERENCES

- BERMAN, N. S. 1989 Polymer contributions to transport equations. In *Drag Reduction in Fluid Flows* (ed. R. H. J. Sellin & R. T. Moses). Ellis Horwood.
- BEWERSDORFF, H. W. 1984 Heterogene Widerslandsverminderung bei Turbulenten Rohrströmungen. *Rheol. Acta* **23**, 522–534.
- BIRD, R. B., CURTISS, C. F., ARMSTRONG, R. C. & HASSAGER, O. 1987 *Dynamics of Polymeric Liquids, vol. 2: Kinetic Theory*, 2nd Edn. Wiley.
- CURTISS, C. F. & BIRD, R. B. 1996 Statistical mechanics of transport phenomena: polymeric liquid mixtures. *Adv. Polymer Sci.* **125**, 1–101.
- DONAHUE, G. L., TIEDERMAN, W. G. & REISCHMANN, M. M. 1972 Flow visualization of the near-wall region in a drag-reducing flow. *J. Fluid Mech.* **56**, 559–575.
- ECKELMAN, L. D., FORTUNA, G. & HANRATTY, T. J. 1972 Drag reduction and the wave length of flow-oriented wall eddies. *Nature* **236**, 94–96.
- FORTUNA, G. & HANRATTY, T. J. 1972 The Influence of drag reducing polymers on turbulence in the viscous sublayer. *J. Fluid Mech.* **53**, 575–586.
- GADD, G. E. 1965 Turbulence damping and drag reduction produced by certain additives in water. *Nature* **206**, 463.
- GENNES, P. G. DE 1990 *Introduction to Polymer Dynamics*. Cambridge University Press.
- HANRATTY, T. J., LYONS, S. L. & MCLAUGHLIN, J. B. 1990 Interpretation of polymer drag reduction in terms of turbulence producing eddies close to a wall. In *Structure of Turbulence and Drag Reduction* (ed. A. Gyr), pp. 407–415. Springer.
- HINZE, J. O. 1987 *Turbulence*, 2nd Edn, pp. 68–72. McGraw-Hill.
- JAMES, D. F., MCLEAN, B. & SARINGER, J. H. 1987 Presheared extensional flow of dilute polymer solutions. *J. Rheol.* **31**, 453.
- KOSKIE, J. E. & TIEDERMAN, W. G. 1991 Polymer drag reduction of a zero-pressure-gradient boundary layer. *Phys. Fluids A* **3**, 2471–2473.
- LIU, T. W. 1989 *J. Chem. Phys.* **90**, 582–592.
- LUCHIK, T. S. & TIEDERMAN, W. G. 1988 Turbulent structure in low-concentration drag-reducing channel flows. *J. Fluid Mech.* **190**, 241–263.
- LUMLEY, J. L. 1969 Drag reduction by additives. *Ann. Rev. Fluid Mech.* **1**, 367–384.
- LUMLEY, J. L. 1973 Drag reduction in turbulent flow by polymer additives. *J. Polymer Sci. Macromol. Rev.* **7**, 263–190.
- LUMLEY, J. L. & KUBO, I. 1984 Turbulent drag reduction by polymer additives: a survey. *IUTAM Symp., Essen, Germany, June 26–28*.
- LYONS, S. L., NIKOLAIDES, C. & HANRATTY, T. J. 1988 The size of turbulent eddies close to a wall. *AIChE J.* **34**, 938.
- MASSAH, H. 1993 Studies of the interaction between drag-reducing polymers and a turbulent flow field using PIV and FENE bead-spring model. PhD thesis, University of Illinois, Urbana.
- MASSAH, H., KONTOMARIS, K., SCHOWALTER, W. R. & HANRATTY, T. J. 1993 The configuration of a FENE bead-spring chain in transient rheological flows and in a turbulent flow. *Phys. Fluids A* **5**, 881–890.
- MERRILL, E. W., SMITH, K. A., SHEN, H. & MICKLEY, H. S. 1966 Study of turbulent flows of dilute polymer solutions in a Couette viscometer. *Trans. Soc. Rheol.* **10**, 335–351.
- METZNER, A. B. & METZNER, A. P. 1970 Stress levels in rapid extensional flows of polymeric fluids. *Rheol. Acta* **9**, 174–181.
- METZNER, A. B. & PARK, M. G. 1964 Turbulent flow characteristics of viscoelastic fluids. *J. Fluid Mech.* **20**, 291–303.
- MIZUSHIMA, T. & USUI, H. 1997 Reduction of eddy diffusion for momentum and heat in viscoelastic fluid flow in a circular tube. *Phys. Fluids Suppl.* **20**, S100.
- MOCHIMARU, Y. 1981 Further comments on the FENE-P dumbbell model. *J. Non-Newtonian Fluid Mech.* **9**, 179.
- NIKOLAIDES, C. 1984 A study of the coherent structures in the viscous wall region of a turbulent flow. PhD thesis, University of Illinois, Urbana.

- OETTINGER, H. C. & WEDGEWOOD, L. 1988 A model of dilute polymer solutions with hydrodynamic interaction and finite extensibility: shear flows. *J. Non-Newtonian Fluid Mech.* **27**, 245–264.
- OLDAKER, D. K. & TIEDERMAN, W. G. 1977 Spatial structure of the viscous sub-layer in drag-reducing channel flows. *Phys. Fluids* **20**, S133–S144.
- PATTERSON, R. W. & ABERNATHY, F. H. 1970 Turbulent flow drag reduction and degradation with dilute polymer solutions. *J. Fluid Mech.* **43**, 689–710.
- PETERLIN, A. 1966 Hydrodynamics of linear macromolecules. *Pure Appl. Chem.* **12**, 273.
- RISEMAN, J. & KIRKWOOD, J. G. 1956 The statistical mechanical theory of irreversible processes in solutions of macromolecules. In *Rheology*, vol. 1 (ed. F. R. Eirich), pp. 510–523. Academic.
- SEYER, F. A. & METZNER, A. B. 1969 Turbulent phenomena in drag reducing systems. *AIChE J.* **15**, 426–434.
- TIEDERMAN, W. G. 1990 The effect of dilute polymer solutions in viscous drag and turbulence structure. In *Structure of Turbulence and Drag Reduction* (ed. A. Gyr), pp. 187–200. Springer.
- TOONDER, J. M. J. DEN 1996 Drag reduction by polymer additives in a turbulent pipe flow: laboratory and numerical experiments. Doctoral thesis, Technische Universiteit Delft.
- USUI, H. 1990 Drag reduction caused by the injection of a polymer solution into a pipe. In *Structure of Turbulence and Drag Reduction* (ed. A. Gyr), pp. 257–274. Springer.
- VIRK, P. S. 1975 Drag reduction fundamentals. *AIChE J.* **21**, 625–656.
- VISSMAN, K. & BEWERSDORFF, H. W. 1989 The influence of pre-shearing on the elongational behavior of drag reducing fluids. In *Drag Reduction in Fluid Flows* (ed. R. H. J. Selin & R. T. Moses), pp. 61–67. Ellis Horwood.
- WALKER, D. T., TIEDERMAN, W. G. & LUCHIK, T. S. 1986 Optimization of the injection process for drag-reducing additives. *Exps. Fluids* **4**, 114.
- WEDGEWOOD, L. E. & BIRD, R. B. 1988 From molecular models to the solutions of flow problems. *I & EC Res.* **27**, 1313–1320.
- WEDGEWOOD, L. E., OSTROY, D. N. & BIRD, R. B. 1991 A finitely extensible bead-spring chain model for dilute polymer solutions. *J. Non-Newtonian Fluid Mech.* **40**, 119–139.
- WIEST, J. M., WEDGEWOOD, L. E. & BIRD, R. B. 1988 On coil-stretch transition in dilute polymer solutions. *J. Chem. Phys.* **90**, 587.
- WILLMARTH, W. W., WEI, T. & LEE, C. O. 1987 Laser anemometer measurements of Reynolds stress in a turbulent channel flow with drag reducing polymer additives. *Phys. Fluids* **30**, 933–935.